ELASTIC IMPACT OF A PENDULUM ON A FRICTIONAL SURFACE

A THESIS SUBMITTED TO
THE DEPARTMENT OF MECHANICAL ENGINEERING
AND THE GRADUATE SCHOOL OF ENGINEERING AND SCIENCE
OF BILKENT UNIVERSITY
IN PARTIAL FULFILLMENT OF THE REQUIREMENTS
FOR THE DEGREE OF
MASTER OF SCIENCE

By
Seyit Can BİRLİK
September, 2012

I certify that I have read this thesis and that in my opinion it is fully adequate, in scope and in quality, as a thesis for the degree of Master of Science.

Prof. Dr. Adnan AKAY(Advisor)

I certify that I have read this thesis and that in my opinion it is fully adequate, in scope and in quality, as a thesis for the degree of Master of Science.

Assist. Prof. Dr. İlker TEMİZER

I certify that I have read this thesis and that in my opinion it is fully adequate, in scope and in quality, as a thesis for the degree of Master of Science.

Prof. Dr. Faruk ARINÇ

Approved for the Graduate School of Engineering and Science:

Prof. Dr. Levent Onural
Director of the Graduate School

ABSTRACT

ELASTIC IMPACT OF A PENDULUM ON A FRICTIONAL SURFACE

Seyit Can BİRLİK
M.S. in Mechanical Engineering
Supervisor: Prof. Dr. Adnan AKAY
September, 2012

Constrained impacts with friction frequently exist in mechanical systems such as robotic arms, hard disk drives and other mechanisms. Such discontinuous contacts, if not designed and analysed properly, can lead to malfunctions. In particular, for the analysis of problems that involve eccentric collisions and reversal of friction force, use of stereomechanical impact theory with coefficient of restitution can produce paradoxical energy increase. Alternatively, continuum models, which provide more detailed analysis for such problems, can be used, however they are computationally tedious. Instead, here, contact is described by compliant elements with friction and applied to a physical pendulum.

In this thesis, impact-momentum relations for general three-dimensional free collisions are modified for a pendulum which exemplifies an impact with friction and constraint. Inclusion of tangential compliance to model enables the model to demonstrate tangential force reversals and their transition between stick and slip, which is demonstrated using a sphere and a slender rod obliquely colliding with a rough massive plane.

Use of compliant elements to describe impact by a planar pendulum produces differences in the behavior of a constrained system compared with free impacts. For instance, in free collisions an impact that starts with an initial sticking, is always followed by sliding. However, in a pendulum if the contact begins by sticking, it continues to stick throughout the duration of impact. Another difference appears when contact starts with an initial sliding. In free impact, sliding is followed by sticking and sliding, then the body rebounds unless the collision is inelastic. However, in the constrained case wedging of the pendulum is observed if initial angle of collision is below a critical value for a specified friction coefficient.

Keywords: impact, collision, constrained impact, impact with friction, pendulum.

ÖZET
SARKACIN SÜRTÜNMELİ BİR YÜZEY İLE ÇARPIŞMASI

Seyit Can BİRLİK
Makine Mühendisliği, Yüksek Lisans
Tez Yöneticisi: Prof. Dr. Adnan AKAY
Eylül, 2012

Hareket yeteneği kısıtlanmış sürtünmeli çarpışmalar, robotik kolları gibi mekanik sistemlerde sıklıkla gözlemlenmektedir. Bunlar gibi devamsızlık gösteren temaslar uygun olarak tasarlanmazsa işlev bozukluklarına yol açabilmektedir. Merkezleri kaçık çarpışma ve sürtünme kuvvetinin yön değiştirdiği bu tarz problemlerin analizlerinde steromekanik çarpışma teorisinin geri getirme katsayısı ile kullanılması paradoksal enerji artışı ile sonuçlanabilir. Alternatif olarak kullanılabilecek, bu çeşit çarpışmalarda daha fazla detay veren sürekli ortam modelleri ise hesaplama açısından zor ve uğraştırıcıdırlar. Bunların yerine, temasın sürtünme ve kompliyant elemanlarla tanımlandığı bir model oluşturulup fiziksel sarkaç üzerinde uygulanmıştır.

Bu tezde, üç boyutlu serbest çarpışmalar için impals-momentum ilişkileri kurulmuş ve bu ilişkiler kısıtlı ve sürtünmenin dahil edildiği bir çarpışmayı örneklendirebilecek sarkaç için düzenlenmiştir. Temasa teğetsel kompliyans eklenmesi, modelin teğetsel kuvvet yön değiştirmelerine ve yapışma-kayma arasında geçiş yapabilmesine olanak sağlamıştır. Çarpışmanın bahsedilen özellikleri ise bir küre ve bir çubuğun eğik olarak sürtünmeli bir yüzeye çarpışmasıyla örneklendirilmiştir.

Kompliyans elementlerin düzelemsel sarkacın çarpışması için kullanılması, serbest çarpışmalara göre farklar yaratmaktadır. Örneğin, yapışmayla başlayan bir serbest çarpışma, her zaman kaymayla sonuçlanmaktadır. Ancak, sarkaçta eğer çarpışma yapışmayla başlıyorsa, çarpışma boyunca bu şekilde devam etmektedir. Bir başka fark da kaymayla başlayan çarpışmalarda görülmektedir. Serbest çarpışmalarda kaymayla başlayan çarpışmayı yapışma ve tekrar kayma fazları takip etmektedir ve eğer çarpışma inelastik değilse çarpan cisim zıplamaktadır. Ancak, kısıtlanmış harekette, eğer belli bir sürtünme katsayısı için çarpma açısı belli bir değerin altındaysa sarkacın sıkışması gözlemlenmektedir.

Anahtar sözcükler: çarpışma, kısıtlı çarpışma, sürtünmeli çarpışma, sarkaç.

Acknowledgement

First and most, I would like to thank Prof. Dr. Adnan Akay for his patience, valuable guidance and advices, without his support I would never have been able to complete this thesis.

I owe sincere and earnest appreciation to Asst. Prof. Ilker Temizer and Prof. Faruk Arınç for evaluating my thesis and their constructive criticisms. I also owe special thanks to Asst. Prof. Melih Çakmakçı and Asst. Prof. Sinan Filiz for their significant contributions to my graduate education.

Life in a new environment is always hard, and I want to thank Emrullah Kormaz, Emre Akgün and Ismail Uyanık for making the M.S. experience memorable for me. I also want to express gratitude to my friends not only supporting me during my graduate education but also making my life more livable.

Last but not least, I want to thank my family, Ahmet, Çağıl and Esen Birlik and my grandparents with all my heart, for their support and encouragement. They always shared my worries and made me feel their love from kilometers away.

Contents

List of Figures

List of Tables

List of Symbols

a_{ij} : elements of effective mass matrix, $\boldsymbol{B}$

d : distance between specified points

e : coefficient of restitution

e_* : energetic coefficient of restitution

k_1 : stiffness in tangential direction

k_3 : stiffness in normal direction

m : mass

s : sliding velocity

$\hat{s}$: sliding direction

u_1 : displacement of the tangential compliant element

$\dot{u}_1$: rate of change of the displacement of the tangential compliant element

u_3 : displacement of the normal compliant element

$\dot{u}_3$: rate of change of the displacement of the normal compliant element

x : distance in n_1 direction

y : distance in n_2 direction

z : distance in n_3 direction

$\dot{x}$: linear velocity in n_1 direction

$\dot{y}$: linear velocity in n_2 direction

$\dot{z}$: linear velocity in n_3 direction

$\boldsymbol{B}$: effective mass matrix

J_{ij} : moment and products of inertia

J_{ij}^{-1} : elements of inverse inertia tensor

L : length of the pendulum

P_i : component of linear impulse vector in i'th direction

R : radius of the sphere

List of Symbols

$\boldsymbol{F}$	: force vector
$\boldsymbol{H}$	: angular impulse vector
$\boldsymbol{J}$	: inertia tensor
$\boldsymbol{J}^{-1}$	: inverse inertia tensor
$\boldsymbol{M}$	:moment vector
$\boldsymbol{V}$	: velocity vector
$\boldsymbol{P}$	: linear impulse vector
μ	: friction coefficient
θ	: impact angle for pendulum, incidence angle for other examples
θ_{cr}	: critical angle for wedging
$\theta_{cr,r}$	: critical angle for wedging with rigid body assumption
$\dot{\theta}$	: angular velocity of the pendulum about n_2, if subscript is not used
$\ddot{\theta}$	:angular acceleration of the pendulum about n_2, if subscript is not used
$\dot{\boldsymbol{\theta}}$	: angular velocity vector
$\boldsymbol{\rho}$	: position vector
ω	: one of the modal frequencies of a system
ω_o	: natural frequency of the system
$\boldsymbol{\Delta}$	: denotes difference
Ω	: one of the modal frequencies of the system
subscripts	
c	: end of the compression phase
f	: end of collision
lt	: sliding to sticking transition for initially sliding impact
n	: normal component of a vector
o	: parameter (distance, moment of inertia etc.) corrected for rotation point O
t	: tangential component of a vector
tl	: sticking to sliding transition for initially sliding impact
σ	: sticking to sliding transition for initially sticking impact

Chapter 1

Introduction

In the analysis of impact problems, one is typically interested in reaction forces and impulses and/or dynamic response of the system to the collision. One may focus only on the impact forces for example, for the purposes of determining whether the colliding bodies deform plastically or to make sure that the colliding components are running under safe conditions. Alternatively, one may focus only on the dynamics of the system to determine how the bodies move following impact to completely understand the coupled nature of impacting system.

Impacting bodies are frequently encountered in engineering applications hence the subject continues to draw attention. Analysis of impact or collision is required for examples such as punch-press appliaction as a manufacturing process, design of vehicles to be able to make sure that the vehicle is safe enough after a car crash, in robotic applications where an arm is moving and colliding in a frictional environment, modeling of intermittent contact of a hard-disk drive, or investigation of the dynamics of a one legged jumping robot. All of these systems and many others, involve discontinuous contacts. In particular, for systems that are constrained, if the impact is frictional, the inherent discontinuity in the system may lead to behavior such as wedging, jamming and swerve that can result in mulfunctioning of the system.

Selection of the solution method for constrained frictional collisions is important because of the mathematical or physical complications in the problems. For example, using coefficient of restitution in classical theory of impact as a ratio of final and initial velocities, causes paradoxical energy increase if the impact is eccentric and frictional [1]. To overcome such problems deformable elements approach is recommended [2]. The latter approach basically consists of placing a deformable massless element at the contact point and using the deformations on that element in calculating forces followed by the dynamic response of the system to these forces. In addition to solving paradoxical phenomena, use of deformable elements method allows inclusion of material properties in the solution unlike the coefficient of restitution and is computationally much faster than when using the continuum models.

Method of deformable elements is extended to oblique impacts using normal and tangential compliant elements at the contact point, by considering the contact condition as sliding and sticking [3]. This compliant element model is able to demonstrate the stick-slip cases and force reversals with relative computational ease compared with the continuum models (e.g. [4]). Application of the compliant elements model to frictional constrained collisions can be best demonstrated by a pendulum, which is a very simple prototypical model and represents the aforementioned engineering systems very well.

In this thesis, an analytical model is constructed for constrained frictional collisions, using tangential and normal compliance elements at the contact point and using a planar pendulum impacting on a massive plane with friction.

Studies related to the problems encountered in constrained collisions with friction will be summarized in the Background and State of the Art in Chapter 2. Then, the thesis starts with a description of free impact of two elastic bodies and presents the derivation of the equations describing their motion during impact and the expression for the relative velocity during contact. In Chapter 3, a detailed review and after a brief summary on frictional impacts, the model of compliant elements at contact is introduced followed by two examples: (i) oblique impact of a free sphere on a massive surface with friction, and (ii) oblique impact of a slender

rod on a massive surface with friction, are presented with compliant elements at the contact interface. Equations derived for free collisions are modified for constrained bodies; where one is assumed to be infinitely large and stationary and the other is a pendulum having one and two degrees of freedom. For a 3D pendulum, change of sliding direction during collision, swerve [3], is analysed. Finally, the model with two compliant elements at the contact interface is applied to a 2D physical pendulum, which represents constrained impact with friction. Both, initially sliding and initially sticking cases and dissipation mechanisms during collision are discussed in detail and wedging phenomenon is analyzsed comparing it with the rigid-body assumption.

Chapter 2

Background and State of the Art

In investigating the impact of a pendulum on a massive plate, consideration of impact mechanisms together with friction between the impacting bodies further complicate the problem. Oblique problem that the pendulum undergoes has been investigated for uncostrained impacts in much detail, using various approaches, described below.

Confining the problem addressed here to low-speed impacts, modeling efforts can be classified as; particle impact, rigid-body impact, transverse impact on flexible bodies and axial impact on flexible bodies [5], or considering continuity of the solution; impulse-momentum (discrete) and continuous [6]. An alternative generalized classification is provided by Ivanov that covers and integrates them all [7] such that:

- Stereomechanical (classical) theory: Deformation of the bodies are neglected and impact is assumed to be instantaneous. Impulse momentum relations are used and (almost always) linear, algebraic equations are obtained [8], which require reasonable computation time. To equalise number of unknowns to number of equations, coefficient of restitution (COR) should be included in the calculations. However, coefficient of restitution, which relates one of the system parameters (velocity, impulse or energy) at two

stages (initial to final or end of compression to end of restitution) of impact, is independent of the physical properties of the colliding bodies [7] and mostly empirically defined. Also, in oblique impacts, inclusion of tangential impulse is problematic, since either Coulomb's law of friction is used -which is discontinuous for some cases- or coefficients like tangential coefficient of restitution is used whose definition is again an uncertain parameter [6]. One other disadvantage of using classical theory in impact is the fact that it is hard to apply this method to the systems with multiple bodies with several contact points [6].

Classical theory is used successfully if detailed time-dependent analysis of contact is not required [8–13]. Many different problems are solved using stereomechanical model, for instance problem of "rolling friction moment" in a constrained rigid body impact [14], problem of frictional impact by dividing the impact into compression and restitution phases and applying stored momenta (in normal and tangential directions) during compression to the restitution phase by considering losses [15] etc.

- Wave impact theory: In this approach, stress waves created by the impact are taken into account. This method is preferred, if the energy transmitted by the waves constitute a significant fraction of the impact energy. Equations derived for general impacts [16] can be used for more general impacts or there are more specific solutions for some cases such as axial impact on slender deformable bodies [5, 17].

  One of the main differences of wave impact theory from other approaches is the energetic losses from elastic impacts due to elastic stress waves [18]. Theoretical and experimental studies try to explain this. For instance, Reed [19] researches the elastic wave propagation with energy dissipation for a impact of an elastic sphere on an elastic massive substrate using Hunter's approximation to the Hertz contact theory, Seifried et al. [20] compare their FEM model with experimental data validating their calculations with impact of a steel sphere to an aluminum rod and compare experimental and numerical results in plastically deformed impacts [21].

- Deformable elements method: In contrast to the above theories, colliding

bodies are neither completely rigid nor the impact affects the whole body. Effect of the collision is limited to a small region. This method has several advantages. Unlike the classical theory, time-dependent forces and displacements can be obtained and computation time is not as high as wave impact theory [2]. On the other hand, if losses due to waves are not negligible or a quick, rough estimation of after collision properties are needed, deformable elements method is not preferable.

Basis of the approach starts with Hertz' contact theory [22] despite the fact that its derivation has static elastic nature [17]. Then, again without considering impacts, tangential compliance is introduced [23, 24] . Afterwards, tangential compliance of materials is used in the oblique impact of spheres [4] and then findings of the study (sticking-sliding distinction during contact, reversal of the tangential force etc.) are validated with experiments [25, 26]. Although aforementioned studies revealed the effect of tangential compliance, the methods were complex and computation time was high, hence studies on simplifications in the calculations were carried on. For instance, Jaeger [27] defined stress as a sum of Catteneo-Mindlin functions instead of discrete set of points which avoided the large set of equations yet obtaining the same results given by Maw et. al. [4]. Several experimental studies have also assesed the effect of tangential compliance. For instance, Garland and Rogers [28] obtained impact waveforms for an oblique impact and compared their results with those of Hertz and other tangential compliance methods. Osakue and Rogers [29] conducted experiments that indicate the stick-slip behavior.

To simplify the calculations made using compliant impact further, placing two compliant elements (normal and tangential) at the contact point was proposed and it was demonstrated that the results were similar to the continuum model proposed by Maw et al. Examples of a collinear impact [3] and an eccentric impact [30] demonstrated the ease and effectiveness of the model. Basically, the model consists of two compliant elements in normal and tangential directions and connects the contact point and rigid body. Angle of incidence of the velocity of the body determines the stick and slip conditions and transition between these conditions.

For the inclusion of friction in impacts by linearly relating frictional impact to the normal impact via coefficient of friction [31], several authors focused on the inconsistency in eccentric frictional impacts showing that Newton's [32] (which is defined as the the ratio of final and initial velocities) and Poisson's (ratio of normal impulses at the end of the impact and at the end of the compression phase) coefficient of restitutions caused violation of energy conservation [33, 34]. Hence, Stronge defined coefficient of restitution as the ratio of the work done during rebound to that during the compression phase (named energetic coefficient of restitution, which is defined in detail in [6,33,35,36]) proving that problems with frictional impacts are overcome. Inconsistencies of Newton's and Poisson's coefficient of restitution in impact with friction and reversal of the tangential force have been investigated in detail. For example, Stronge [1] compares the approaches from an energy dissipation view, Batlle [37] defines conditions for Newton's and Poisson's coefficient of restitution to be energetically consistent, Ivanov [38] shows that Newton's approach can validate the conservation of energy, and Poisson's approach gives higher energy dissipation than the experimental values, and claims that energetic coefficient of restitution is more realistic. Lubarda [36] defines the boundaries of approaches using impact of a rigid pendulum. Brach extended the COR concept beyond the normal motion of the impacting bodies, defining tangential COR that acts like coefficient of friction [10] and defined COR for moment in [12].

Inclusion of coefficient of friction as defined by Coulomb is commonly used in conventional approaches, wave impact theory, and deformable elements method. For instance, Keller [39] uses normal impulse to parametrize the impact with the help of Poisson's coefficient of restitution and Coulomb's friction. Brach [11] calculates the differences in tangential velocity using tangential impulse and relates this to normal impulse with coefficient of friction. In deformable elements method, Amontons-Coulomb type friction force is again included if the bodies are sliding (e.g. in [3, 4, 30, 40]). For a good review of the methods other than Amontons-Coulomb law that are used in contact problems are given in [41].

Another common dissipation mechanism is damping. Simplest model that includes damping in collision is a linear spring dashpot model in normal direction

[17]. As an other example, Hess and Soom [42] model contact under harmonic loads using a non-linear spring and viscous damper. Lankarani and Nikravesh [43] uses a hysteresis damping function for the losses among with the Hertzian contact.

Another important phenomenon in the pendulum problem is the obliquity of the impact. It adds significant complexity to the problem by introducing a tangential component to the velocity. Because of the tangential component of the velocity, pendulum is exposed to tangential impulse, giving rise to sliding-sticking, direction of sliding and reversal of tangential force during contact.

Studies related to oblique impact start with the analysis of normal impact, which begins with Hertz theory. Detailed analysis of Hertz' work and following advances in this topic is reported by Johnson [44]. In a more detailed analysis of normal impact based on theory of Hertz, Zener uses impact forces to calculate transverse displacements and then relates this to COR [45]. Hunter shows that, this approach can be used for impact of a sphere on a thick plate [18]. Villaggio [46] uses an elastic solution for the normal impact of a sphere considering elastic waves and finds slightly higher duration of impact then Hertz. Chang and Ling [47] use an elastic-plastic model for normal impacts which is dependent on surface and material properties in addition to initial velocity and compare their results with other works.

As mentioned, oblique impacts involve challenging phenomena due to complexity of friction and tangential compliance in the contacting bodies. The solution for tangential compliance was introduced by Mindlin in [23] reporting that tangential displacements are dependent on the previous load history. Mindlin also considered micro-slip regions and showed that even when the tangential force is less then the friction force there are stuck regions as well as sliding regions in the contact area. Stick-slip transition during contact was extended for oblique impacts by Maw et al. [4] who showed that the contact area is divided into concentric annuli to find sticking and sliding regions. The results show that rigid-body approach is not appropriate except for low and high angles of incidence. Their study aslo showed the importance of compliance in oblique impacts. Maw et al. [25, 26] validated their findings with experiments. Garland and Rogers [48] argue that

one can obtain similar results with Maw et al. using shear stress distribution to calculate tangential force with decreased computation time. Jaeger [27] obtains analytical solutions for normal and tangential impact and torsional moment.

In order to simplify the aforementioned complex solutions for oblique impact, some authors solve the problem with normal and tangential compliant elements attached between contact point and the body [2, 3, 7, 30, 49]. In this approach set of differential equations in normal and tangential directions at the contact point are solved as a function of displacement and its derivatives. From displacements, forces and impulses can be calculated as a function of time. Lim and Stronge [50] use the same model in elastic-plastic impact and compare the results with the results of a FEM model and shows that the results are in very good agreement.

Among the experimental investigations of normal and oblique impact studies, Goldsmith [17] presents many experimental results for normal impacts which shows COR, contact duration, contact diameter for different impact cases. Gugan [51] reports on experiments with similar results as the theoretical work of Hertz in spite of the plastic deformations encountered during the tests. Gorham and Kharaz [52] reported test with aluminium spheres colliding with a thick platel and find similar results with numerical work of Maw et al. Osakue and Rogers [29] conducted tests of oblique impact using a pendulum and shows the stick-slip and gross-slip phenomena really exists during oblique impacts. Seireg and Waiter [53] use a pendulum to find the friction coefficient and kinetic coefficient during impact. Shi and Polycarpou [54] runs experiments to find contact stiffness and material damping values using realistic rough surface and compares these with the findings of Hertz. Hutchings et al. [54] report experiments with oblique impact of hard sphere to ductile surface and presents results with analytical solutions.

Almost all of the aforementioned studies consider planar impacts, however there are also several publications related to three-dimensional impacts of bodies. For example, Jia [55] extends Stronge's works in [3, 30] to 3D impact using three orthogonal springs and by considering stick-slip transitions derives solution. Non-planar changes in velocity during 3D impact are analysed in detail by several authors. Stronge investigates the concept of swerve [40] that develops during

frictional impact and defines critical angles for it. Bhatt and Koechling [56–58] refers to swerve, the change of direction of velocity, as flow and find invariant directions, flow change directions and show possible flow patterns, sticking and sliding conditions using rigid body dynamics. In these studies the central aim is to predict the qualitative behavior of the impacting bodies and applying these patterns to numerical calculations. Battle [59] uses a similar approach to find the dependence of the flow to friction coefficient and other parameters. Zhen and Liu [60] find solutions for 3D impacts using normal impulse as a differential variable and solving the differential equations with a numerical method and solves examples with this method.

Nearly all of the studies highlighted above deal with impacts of free bodies or derivation of equations for general collisions. Their application to constrained motions, such as that by a pendulum, brings additional challanges. Some of these are described in several studies. For instance, Lubarda [36] discusses the bounds for different types of coefficients of restitution, Marghitu and Stoenescu [14] discuss the effects of moment rolling friction, Pfieffer and Glocker [15] discusses the frictional impact, Zhen and Liu [60] solve 3D impact problem using pendulum with rigid body assumptions. Constrained impact has specific conditions like wedging (also referred as cut-off, stick), which is physically a locking of the system. Ivanov [7] addresses this issue and offers solutions for cut-off type collisions for a pendulum with springs at the contact point and at its hinge. Stronge [5] uses a similar example to show a collision with multiple contact points neglecting friction. Brach [11] derives equations for a pendulum to make an example of 3D impact however he uses the classical approach.

In the next chapter, a detailed review of the derivation of equations of motion for a free 3D collision is presented. After a brief discussion of frictional impacts, unconstrained collisions in 3D are analysed by reviewing the contact model with compliant elements between the body and the contact body.

Chapter 3

Unconstrained Collisions

In this chapter impact of two free bodies will be discussed and related equations will be derived. Then, after discussing the effect of friction on impacts, free body impact relations will be used in two-dimensional collision models where the second body is a static massive plane.

3.1 Unconstrained Collisions in 3D

According to Newton's second law, a body with mass, m, accelerates with resultant forces, $\mathbf{F}$, on it

$$\frac{d(m\mathbf{V})}{dt} = \mathbf{F} \tag{3.1}$$

similarly, for rotational motion, resultant moments, $\mathbf{M}$, on the body with inertia matrix, $\mathbf{J}$, causes changes in angular acceleration

$$\frac{d(\mathbf{J}\dot{\boldsymbol{\theta}})}{dt} = \mathbf{M} \tag{3.2}$$

Equations (3.1) and (3.2) change the linear and angular velocities of the body and constitute the basis of the impulse-momentum relations. Defining linear momentum as $m\mathbf{V}$ and angular momentum as $\mathbf{J}\dot{\theta}$, by integrating the above equations (assuming inertia properties, m and $\mathbf{J}$ of the body remain constant) the following

relations are obtained:

$$m\boldsymbol{\Delta}\mathbf{V} = \int \mathbf{F}dt \tag{3.3}$$

$$\mathbf{J}\boldsymbol{\Delta}\dot{\boldsymbol{\theta}} = \int \mathbf{M}dt \tag{3.4}$$

Defining linear, $\boldsymbol{P}$ and angular impulses, $\boldsymbol{H}$,respectively, as

$$\mathbf{P} = \int \mathbf{F}dt \tag{3.5}$$

$$\mathbf{H} = \int \mathbf{M}dt \tag{3.6}$$

impulse-momentum relations can be written

$$\mathbf{P} = m\boldsymbol{\Delta}\mathbf{V} \tag{3.7}$$

$$\mathbf{H} = \mathbf{J}\boldsymbol{\Delta}\dot{\boldsymbol{\theta}} \tag{3.8}$$

The linear momenta about the center of mass G, can be used to find the corresponding angular momentum such that

$$\mathbf{H} = \boldsymbol{\rho} \times m\mathbf{V}$$

$$\mathbf{H} = \boldsymbol{\rho} \times \mathbf{P} \tag{3.9}$$

where $\boldsymbol{\rho}$ represents position vector from center of mass G to the contact point C. The relations (3.7) and (3.8) simply mean that if impulse, $\mathbf{P}$, is applied on a body with mass, m, initial velocity of the body is changed by $\boldsymbol{\Delta}\mathbf{V}$, with a similar relationship between angular impulse and velocity.

Invoking Newton's third law and denoting the second body with a prime,

$$\mathbf{F}' = -\mathbf{F} \tag{3.10}$$

$$\mathbf{M}' = -\mathbf{M} \tag{3.11}$$

which leads to the relations of the linear and angular impulses acting on the bodies. Applying this to Equations (3.7) and (3.8) for collision of two bodies

$$m\boldsymbol{\Delta}\mathbf{V} = \mathbf{P}$$

$$m'\boldsymbol{\Delta}\mathbf{V}' = -\mathbf{P}' \tag{3.12}$$

$$\mathbf{J}\Delta\dot{\boldsymbol{\theta}} = \boldsymbol{\rho} \times \mathbf{P} \tag{3.13}$$

$$\mathbf{J}'\Delta\dot{\boldsymbol{\theta}}' = -\boldsymbol{\rho} \times \mathbf{P} \tag{3.14}$$

Linear velocities of the bodies at the contact point, C, are:

$$\mathbf{V_C} = \mathbf{V} + \dot{\boldsymbol{\theta}} \times \boldsymbol{\rho} \tag{3.15}$$

$$\mathbf{V_C}' = \mathbf{V}' + \dot{\boldsymbol{\theta}}' \times \boldsymbol{\rho}' \tag{3.16}$$

relative velocity at the contact point can then be found as

$$\mathbf{V_R} = \mathbf{V_C} - \mathbf{V_C'} = \Big(\mathbf{V} + \dot{\boldsymbol{\theta}} \times \boldsymbol{\rho}\Big) - \Big(\mathbf{V}' + \dot{\boldsymbol{\theta}}' \times \boldsymbol{\rho}'\Big) \tag{3.17}$$

To calculate the change in relative velocity under impulses, consider use of the change of the velocities for each body at the contact point, C,

$$\Delta\mathbf{V_R} = \Big(\Delta\mathbf{V} + \Delta\dot{\boldsymbol{\theta}} \times \boldsymbol{\rho}\Big) - \Big(\Delta\mathbf{V}' + \Delta\dot{\boldsymbol{\theta}}' \times \boldsymbol{\rho}'\Big) \tag{3.18}$$

Rearranging terms

$$\Delta\mathbf{V_R} = (\Delta\mathbf{V} - \Delta\mathbf{V}') + \Big(\Delta\dot{\boldsymbol{\theta}} \times \boldsymbol{\rho} - \Delta\dot{\boldsymbol{\theta}}' \times \boldsymbol{\rho}'\Big) \tag{3.19}$$

using Equations (3.7, 3.12-3.14) produces relative velocity in terms of applied impulses

$$\Delta\mathbf{V_R} = \left(\frac{\mathbf{P}}{m} - \frac{\mathbf{P}'}{m'}\right) + \Big(\mathbf{J}^{-1}(\boldsymbol{\rho} \times \mathbf{P}) \times \boldsymbol{\rho} - \mathbf{J}'^{-1}(\boldsymbol{\rho}' \times \mathbf{P}') \times \boldsymbol{\rho}'\Big) \tag{3.20}$$

In the following sections, terms related to second body will be dropped for simplicity, assuming, the second body is a massive static body (e.g. impact of a free sphere on a massive surface, terms related to second body cancel due to zero velocity). As a result, relative velocity at the contact point becomes

$$\Delta\mathbf{V_R} = m^{-1}\mathbf{P} + \mathbf{J}^{-1}(\boldsymbol{\rho} \times \mathbf{P}) \times \boldsymbol{\rho} \tag{3.21}$$

where the inertia matrix is

$$\mathbf{J} = \begin{bmatrix} J_{11} & J_{12} & J_{13} \\ J_{21} & J_{22} & J_{23} \\ J_{31} & J_{32} & J_{33} \end{bmatrix} \tag{3.22}$$

and the elements of the inverse of J matrix are

$$\mathbf{J}^{-1} = \begin{bmatrix} J_{11}^{-1} & J_{12}^{-1} & J_{13}^{-1} \\ J_{21}^{-1} & J_{22}^{-1} & J_{23}^{-1} \\ J_{31}^{-1} & J_{32}^{-1} & J_{33}^{-1} \end{bmatrix} \tag{3.23}$$

Aligning Cartesian coordinates $\mathbf{n_1}$ and $\mathbf{n_2}$ with the tangential contact plane and $\mathbf{n_3}$ as the normal to that plane, vectorial position from point of rotation to contact point in directions $\mathbf{n_1}$, $\mathbf{n_2}$ and $\mathbf{n_3}$ are denoted by x, y and z, respectively. Then, the position vector, $\boldsymbol{\rho}$, becomes

$$\boldsymbol{\rho} = \begin{bmatrix} x \\ y \\ z \end{bmatrix} \tag{3.24}$$

and components of impulse vector are

$$\mathbf{P} = \begin{bmatrix} P_1 \\ P_2 \\ P_3 \end{bmatrix} \tag{3.25}$$

Substituting Equations (3.22-3.25) gives direct relation between $\mathbf{\Delta V_R}$ and $\mathbf{P}$ presenting a more compact form. From Equation (3.21)

$$\mathbf{\Delta V_R} = m^{-1} \begin{bmatrix} P_1 \\ P_2 \\ P_3 \end{bmatrix} + \mathbf{J}^{-1} \left(\begin{bmatrix} x \\ y \\ z \end{bmatrix} \times \begin{bmatrix} P_1 \\ P_2 \\ P_3 \end{bmatrix} \right) \times \begin{bmatrix} x \\ y \\ z \end{bmatrix} \tag{3.26}$$

$$\mathbf{\Delta V_R} = m^{-1} \begin{bmatrix} P_1 \\ P_2 \\ P_3 \end{bmatrix} + \underbrace{\mathbf{J^{-1}} \begin{bmatrix} yP_3 - zP_2 \\ zP_1 - xP_3 \\ xP_2 - yP_1 \end{bmatrix}}_{\mathbf{A}} \times \begin{bmatrix} x \\ y \\ z \end{bmatrix} \tag{3.27}$$

$$\mathbf{A} = \begin{bmatrix} J_{11}^{-1} & J_{12}^{-1} & J_{13}^{-1} \\ J_{21}^{-1} & J_{22}^{-1} & J_{23}^{-1} \\ J_{31}^{-1} & J_{32}^{-1} & J_{33}^{-1} \end{bmatrix} \underbrace{\begin{bmatrix} yP_3 - zP_2 \\ zP_1 - xP_3 \\ xP_2 - yP_1 \end{bmatrix}}_{\begin{bmatrix} a_1 \\ a_2 \\ a_3 \end{bmatrix}} \tag{3.28}$$

$$\mathbf{A} = \begin{bmatrix} J_{11}^{-1}a_1 + J_{12}^{-1}a_2 + J_{13}^{-1}a_3 \\ J_{21}^{-1}a_1 + J_{22}^{-1}a_2 + J_{23}^{-1}a_3 \\ J_{31}^{-1}a_1 + J_{32}^{-1}a_2 + J_{33}^{-1}a_3 \end{bmatrix} \tag{3.29}$$

$$\mathbf{\Delta V_R} = m^{-1} \begin{bmatrix} P_1 \\ P_2 \\ P_3 \end{bmatrix} + \mathbf{A} \times \begin{bmatrix} x \\ y \\ z \end{bmatrix} \tag{3.30}$$

$$\mathbf{\Delta V_R} = m^{-1} \begin{bmatrix} P_1 \\ P_2 \\ P_3 \end{bmatrix} + \begin{bmatrix} \left(J_{21}^{-1}a_1 + J_{22}^{-1}a_2 + J_{23}^{-1}a_3\right) z - \left(J_{31}^{-1}a_1 + J_{32}^{-1}a_2 + J_{33}^{-1}a_3\right) y \\ \left(J_{31}^{-1}a_1 + J_{32}^{-1}a_2 + J_{33}^{-1}a_3\right) x - \left(J_{11}^{-1}a_1 + J_{12}^{-1}a_2 + J_{13}^{-1}a_3\right) z \\ \left(J_{11}^{-1}a_1 + J_{12}^{-1}a_2 + J_{13}^{-1}a_3\right) y - \left(J_{21}^{-1}a_1 + J_{22}^{-1}a_2 + J_{23}^{-1}a_3\right) x \end{bmatrix} \tag{3.31}$$

$$\mathbf{\Delta V_R} = m^{-1} \begin{bmatrix} P_1 \\ P_2 \\ P_3 \end{bmatrix} + \begin{bmatrix} \left(J_{21}^{-1}z - J_{31}^{-1}y\right) a_1 + \left(J_{22}^{-1}z - J_{32}^{-1}y\right) a_2 + \left(J_{23}^{-1}z - J_{33}^{-1}y\right) a_3 \\ \left(J_{31}^{-1}x - J_{11}^{-1}z\right) a_1 + \left(J_{32}^{-1}x - J_{12}^{-1}z\right) a_2 + \left(J_{33}^{-1}x - J_{13}^{-1}z\right) a_3 \\ \left(J_{11}^{-1}y - J_{21}^{-1}x\right) a_1 + \left(J_{12}^{-1}y - J_{22}^{-1}x\right) a_2 + \left(J_{13}^{-1}y - J_{23}^{-1}x\right) a_3 \end{bmatrix} \tag{3.32}$$

$$\mathbf{\Delta V_R} = m^{-1} \begin{bmatrix} P_1 \\ P_2 \\ P_3 \end{bmatrix} +$$

$$\begin{bmatrix} \left(J_{21}^{-1}z - J_{31}^{-1}y\right)(yP_3 - zP_2) + \left(J_{22}^{-1}z - J_{32}^{-1}y\right)(zP_1 - xP_3) + \left(J_{23}^{-1}z - J_{33}^{-1}y\right)(xP_2 - yP_1) \\ \left(J_{31}^{-1}x - J_{11}^{-1}z\right)(yP_3 - zP_2) + \left(J_{32}^{-1}x - J_{12}^{-1}z\right)(zP_1 - xP_3) + \left(J_{33}^{-1}x - J_{13}^{-1}z\right)(xP_2 - yP_1) \\ \left(J_{11}^{-1}y - J_{21}^{-1}x\right)(yP_3 - zP_2) + \left(J_{12}^{-1}y - J_{22}^{-1}x\right)(zP_1 - xP_3) + \left(J_{13}^{-1}y - J_{23}^{-1}x\right)(xP_2 - yP_1) \end{bmatrix}$$

$$\mathbf{\Delta V_R} = m^{-1} \begin{bmatrix} P_1 \\ P_2 \\ P_3 \end{bmatrix} + \begin{bmatrix} A_1 + A_2 + A_3 \\ A_4 + A_5 + A_6 \\ A_7 + A_8 + A_9 \end{bmatrix} \tag{3.33}$$

where:

$$
\begin{aligned}
A_1 &= \left(J_{21}^{-1} zyP_3 - J_{21}^{-1} z^2 P_2 - J_{31}^{-1} y^2 P_3 + J_{31}^{-1} yzP_2\right) \\
A_2 &= \left(J_{22}^{-1} z^2 P_1 - J_{22}^{-1} zxP_3 - J_{32}^{-1} yzP_1 + J_{32}^{-1} yxP_3\right) \\
A_3 &= \left(J_{23}^{-1} zxP_2 - J_{23}^{-1} zyP_1 - J_{33}^{-1} yxP_2 + J_{33}^{-1} y^2 P_1\right) \\
A_4 &= \left(J_{31}^{-1} xyP_3 - J_{31}^{-1} xzP_2 - J_{11}^{-1} zyP_3 + I_{11}^{-1} z^2 P_2\right) \\
A_5 &= \left(J_{32}^{-1} xzP_1 - J_{32}^{-1} x^2 P_3 - J_{12}^{-1} z^2 P_1 + J_{12}^{-1} zxP_3\right) \\
A_6 &= \left(J_{33}^{-1} x^2 P_2 - J_{33}^{-1} xyP_1 - J_{13}^{-1} zxP_2 + J_{13}^{-1} zyP_1\right) \\
A_7 &= \left(J_{11}^{-1} y^2 P_3 - J_{11}^{-1} yzP_2 - J_{21}^{-1} xyP_3 + J_{21}^{-1} xzP_2\right) \\
A_8 &= \left(J_{12}^{-1} yzP_1 - J_{12}^{-1} yxP_3 - J_{22}^{-1} xzP_1 + J_{22}^{-1} x^2 P_3\right) \\
A_9 &= \left(J_{13}^{-1} yxP_2 - J_{13}^{-1} y^2 P_1 - J_{23}^{-1} x^2 P_2 + J_{23}^{-1} xyP_1\right)
\end{aligned}
$$

$$\boldsymbol{\Delta V_R} = \begin{bmatrix} \left(m^{-1} + J_{22}^{-1}z^2 - J_{32}^{-1}yz - J_{23}^{-1}zy + J_{33}^{-1}y^2\right)P_1 + \left(-J_{21}^{-1}z^2 + J_{31}^{-1}yz + J_{23}^{-1}zx - J_{33}^{-1}yx\right)P_2 + \left(J_{21}^{-1}zy - J_{31}^{-1}y^2 - J_{22}^{-1}zx + J_{32}^{-1}yx\right)P_3 \\ \left(J_{32}^{-1}zx - J_{12}^{-1}z^2 - J_{33}^{-1}xy + J_{13}^{-1}zy\right)P_1 + \left(m^{-1} + -J_{31}^{-1}xz + J_{11}^{-1}z^2 + J_{33}^{-1}x^2 - J_{13}^{-1}zx\right)P_2 + \left(J_{31}^{-1}xy - J_{11}^{-1}zy - J_{32}^{-1}x^2 + J_{12}^{-1}zx\right)P_3 \\ \left(J_{12}^{-1}yz - J_{22}^{-1}xz - J_{13}^{-1}y^2 + J_{23}^{-1}xy\right)P_1 + \left(-J_{11}^{-1}yz + J_{21}^{-1}xz + J_{13}^{-1}yx - J_{23}^{-1}x^2\right)P_2 + \left(m^{-1} + J_{11}^{-1}y^2 - J_{21}^{-1}xy - J_{12}^{-1}xy + J_{22}^{-1}x^2\right)P_3 \end{bmatrix} \tag{3.34}$$

$$\boldsymbol{\Delta V_R} = \underbrace{\begin{bmatrix} m^{-1} + J_{22}^{-1}z^2 - J_{32}^{-1}yz - J_{23}^{-1}zy + J_{33}^{-1}y^2 & -J_{21}^{-1}z^2 + J_{31}^{-1}yz + J_{23}^{-1}zx - J_{33}^{-1}yx & J_{21}^{-1}zy - J_{31}^{-1}y^2 - J_{22}^{-1}zx + J_{32}^{-1}yx \\ J_{32}^{-1}zx - J_{12}^{-1}z^2 - J_{33}^{-1}xy + J_{13}^{-1}zy & m^{-1} + -J_{31}^{-1}xz + J_{11}^{-1}z^2 + J_{33}^{-1}x^2 - J_{13}^{-1}zx & J_{31}^{-1}xy - J_{11}^{-1}zy - J_{32}^{-1}x^2 + J_{12}^{-1}zx \\ J_{12}^{-1}yz - J_{22}^{-1}xz - J_{13}^{-1}y^2 + J_{23}^{-1}xy & -J_{11}^{-1}yz + J_{21}^{-1}xz + J_{13}^{-1}yx - J_{23}^{-1}x^2 & m^{-1} + J_{11}^{-1}y^2 - J_{21}^{-1}xy - J_{12}^{-1}xy + J_{22}^{-1}x^2 \end{bmatrix}}_{B} \begin{bmatrix} P_1 \\ P_2 \\ P_3 \end{bmatrix} \tag{3.35}$$

$$\mathbf{B} = \begin{bmatrix} m^{-1} + J_{22}^{-1}z^2 - J_{32}^{-1}yz - J_{23}^{-1}zy + J_{33}^{-1}y^2 & -J_{21}^{-1}z^2 + J_{31}^{-1}yz + J_{23}^{-1}zx - J_{33}^{-1}yx & J_{21}^{-1}zy - J_{31}^{-1}y^2 - J_{22}^{-1}zx + J_{32}^{-1}yx \\ J_{32}^{-1}zx - J_{12}^{-1}z^2 - J_{33}^{-1}xy + J_{13}^{-1}zy & m^{-1} + -J_{31}^{-1}xz + J_{11}^{-1}z^2 + J_{33}^{-1}x^2 - J_{13}^{-1}zx & J_{31}^{-1}xy - J_{11}^{-1}zy - J_{32}^{-1}x^2 + J_{12}^{-1}zx \\ J_{12}^{-1}yz - J_{22}^{-1}xz - J_{13}^{-1}y^2 + J_{23}^{-1}xy & -J_{11}^{-1}yz + J_{21}^{-1}xz + J_{13}^{-1}yx - J_{23}^{-1}x^2 & m^{-1} + J_{11}^{-1}y^2 - J_{21}^{-1}xy - J_{12}^{-1}xy + J_{22}^{-1}x^2 \end{bmatrix} \tag{3.36}$$

$$\boldsymbol{\Delta V_R} = \mathbf{BP} \tag{3.37}$$

For simplicity, in the remainder of this thesis, the elements of B matrix will be represented as follows:

$$\boldsymbol{B} = \begin{bmatrix} a_{11} & a_{12} & a_{13} \\ a_{21} & a_{22} & a_{23} \\ a_{31} & a_{32} & a_{33} \end{bmatrix} \tag{3.38}$$

3.2 Impact with Friction

Friction is a resistive force due to relative motion or intended relative motion of objects. In this thesis friction refers to dry friction, which is often classified as static and kinetic friction. These two types of friction are assumed to be equal for simplicity (for example see [7,30]) and this assumption will be used in throughout the thesis.

According to Amontons-Coulomb friction law, during relative motion of bodies, normal force and friction forces are linearly dependent via a coefficient of friction, μ. This can be expressed as

$$|F_t| = \mu F_n \leftrightarrow \sqrt{V_1^2 + V_2^2} > 0 \tag{3.39}$$

Equation (3.39) is valid if sliding (relative motion) exist (note that $\sqrt{V_1^2 + V_2^2}$ represents the magnitude of the velocity on the tangential contact plane which is the sliding velocity). Remembering the assumption about equality of static and kinetic frictions, if tangential force can not exceed the friction force, relative motion can not develop at the contact point which can be summarized as:

$$|F_t| < \mu F_n \leftrightarrow \sqrt{V_1^2 + V_2^2} = 0 \tag{3.40}$$

These relations can be extended to impact with friction and the normal and tangential impulses can be related through Amontons-Coulomb law (see for example [15, 17]). The resulting relations will be used to explain the stick-slip phenomena during oblique impact in the following sections of the thesis.

Frictional impact requires more detailed and careful analysis due to its comlex nature such as dependence on sliding direction, possibility of violation of energy conservation and locking of the system especially in constrained collision etc. In the impact of a pendulum, these topics will be discussed in detail.

3.3 Unconstrained Collisions in 2D

3.3.1 Collision Models

In the Chapter 2, collision models are classified and discussed in detail, describing their advantages and disadvantages. In this thesis, a type of "deformable elements method" is used where two compliant elements are placed between the contact point and the body because of its aforementioned advantages over other methods. Following sections describe the model in detail and present two examples of collisions of unconstrained bodies using this approach. Then, in the final chapter this model is extended for a constrained impact applying it to a pendulum.

3.3.1.1 Compliant Elements at the Contact

Although many approaches in impact problem neglect tangential compliance, its existence during contact has been validated by experiments and analytical methods [4, 23, 25, 52]. Johnson [16] derived equations showing the compliance of materials and relates tangential compliance to the normal via Poisson's ratio. These studies have shown that the contacting bodies act like springs (in the elastic region, of course) not only in normal direction [44] but also in tangential direction [23]. Maw et al. [4] showed the effects of tangential compliance on oblique impact through a time-dependent solution of contact and illustrate the reversal in slip direction for small angles of incidence and demonstrated it with experiments [25, 26]. They showed that, for a range of initial impact velocities, slip reversal may occur due to tangential compliance. Since classical impact theory neglects tangential compliance, reversal can develop under those conditions. Effects of tangential compliance have been validated experimentally by others for example see [29, 52, 61].

Stronge simplified the approach of Maw et al. using compliant elements [3,30], which will be explained in detail with two examples that Stronge presented in

[3, 30] before applying the method to the problem of impact of a pendulum with friction.

To be able to represent slip reversal, work of Maw et al. [4] is simplified by using normal and tangential compliant elements between the contact point and the body. Stick and slip conditions are derived as a function of the ratio of normal and tangential components of initial impact velocity. Microslip regions used by Mindlin [23] and Maw et al. [4] are neglected, hence the contact point is assumed to either stick or slip. Using equations of motion and Amontons-Coulomb law, dynamics of the impact according to phase of contact (stick or slip) are obtained as a function of time. It was noted that [3] the results are in very good agreement with Maw et al. and capture the basis of slip reversal.

The concept of compliant element model is applied to impact of a sphere (example of collinear impact) [3] and oblique impact of an inclined rod [30] (example of eccentric impact) to demonstrate the results of the model and the model will be explained in detail to consitute the foundation of the approach before applying it to the pendulum problem. First, general 2D equations will be derived and they will be used in the aforementioned examples.

3.3.1.1.1 Dynamics of Collision Considering both linear and angular motion of the body, equations of motion can be written in matrix form as in Equation (3.37) using the **B** matrix:

$$\left\{ \begin{array}{c} d^2x/dt^2 \\ d^2z/dt^2 \end{array} \right\} = \left[\begin{array}{cc} a_{11} & a_{13} \\ a_{31} & a_{33} \end{array} \right] \left\{ \begin{array}{c} F_1 \\ F_3 \end{array} \right\} \tag{3.41}$$

If the impact is eccentric, force-acceleration relation is coupled, i.e. a_{13}, $a_{21} \neq 0$. In explicit form

$$\frac{d^2x}{dt^2} = (a_{11}F_1 + a_{13}F_3) \tag{3.42}$$

$$\frac{d^2z}{dt^2} = (a_{31}F_1 + a_{33}F_3) \tag{3.43}$$

In the following sections, impact will be assumed as perfectly elastic.

3.3.1.1.2 Force Displacement Relation In the compliant elements model normal and tangential springs are assumed to be attached between the contact point C and the body. The compression or elongation of these springs in normal and tangential directions are represented with u_3 and u_1, respectively. The change in length of the springs corresponds to the forces applied at point C, and can be related linearly such that;

$$F_1 = -k_1 u_1 \tag{3.44}$$

$$F_3 = -k_3 u_3 \tag{3.45}$$

where k_1 and k_3 are spring coefficients in tangential and normal directions respectively.

3.3.1.1.3 Sticking or Sliding during Impact Studies of Maw et al. [4] showed that, in an oblique impact, body initially sticks or slides depending on the incidence angle. In [4], sliding refers to the contact region having non-zero relative velocity. In this case, normal and tangential forces can be modelled using Amontons-Coulomb law, i.e. $|F_1| = \mu F_3$. On the other hand, during sticking some of the contacting points have zero relative velocity although the outer zone encircling them may be sliding, describing microslip. This type of compliance effect is neglected during rigid-body calculations.

3.3.1.1.4 Sticking If the tangential force exerted on the body does not exceed sliding friction force, μF_3, the massless particle sticks (i.e attaches) to the surface of the stationary body;

$$|F_1| < \mu F_3 \tag{3.46}$$

During sticking, the tangential velocity, $\dot{x}$, of the body and the rate of change of displacement, $\dot{u}_1$, of the spring are equal. Hence forces in the equation of motion can be related to displacements using $d^2x/dt^2 = d^2u_1/dt^2$. Combining Equations (3.42), (3.43) with (3.44) and (3.45) produces

$$\frac{d^2u_1}{dt^2} = \left[a_{11}\left(-k_1 u_1\right) + a_{13}\left(-k_3 u_3\right)\right]$$

$$\frac{d^2u_3}{dt^2} = \left[a_{13}\left(-k_1u_1\right) + a_{33}\left(-k_3u_3\right)\right]$$

Rewriting in matrix form

$$\left\{ \begin{array}{c} d^2x/dt^2 \\ d^2z/dt^2 \end{array} \right\} = \left\{ \begin{array}{c} d^2u_1/dt^2 \\ d^2u_3/dt^2 \end{array} \right\} = \left[\begin{array}{cc} -a_{11}k_1 & -a_{13}k_3 \\ -a_{31}k_1 & -a_{33}k_3 \end{array} \right] \left\{ \begin{array}{c} u_1 \\ u_3 \end{array} \right\} \tag{3.47}$$

3.3.1.1.5 Sliding If the tangential force exerted on the body overcomes μF_3, contact point of the body slides on the surface of the stationary body. During sliding, Amontons-Coulomb law can be used, hence tangential force can be related to normal force via

$$F_1 = -\mu\hat{s}F_3 \tag{3.48}$$

where $\hat{s} = sign(\dot{x} - \dot{u}_1)$ and shows the direction of sliding and μ is the friction coefficient.

Regardless of the horizontal condition of the body (stick or slip), the rate of change of the normal spring's displacement is equal to relative normal velocity of the body, $\dot{u}_3 = \dot{z}$.

Subtituting Equation (3.48) in Equation (3.43)

$$\frac{d^2z}{dt^2} = \left(-a_{31}\mu\hat{s}F_3 + a_{33}F_3\right)$$

from Equation (3.45)

$$\frac{d^2z}{dt^2} = \left(a_{31}\mu\hat{s} - a_{33}\right)k_3u_3$$

since $\dot{u}_3 = \dot{z}$, equation becomes

$$\frac{d^2u_3}{dt^2} = m^{-1}\left(a_{31}\mu\hat{s} - a_{33}\right)k_3u_3 \tag{3.49}$$

Solution of the differential equation (3.49) with proper initial conditions gives normal displacement of the spring and normal velocity of the body. u_1 and $\dot{u}_1$ can be found by making use of the Amontons-Coulomb law and Equations (3.44) and (3.45).

$$-k_1u_1 = \mu\hat{s}k_3u_3$$

$$u_1 = -\frac{k_3}{k_1}\mu\hat{s}u_3 \tag{3.50}$$

differentiating Equation (3.50) once yields

$$\dot{u}_1 = -\frac{k_3}{k_1}\mu\hat{s}\dot{u}_3 \tag{3.51}$$

3.3.1.1.6 Initially Sticking or Sliding During impact, the body may undergo a sliding or sticking phase. These may follow each other or one phase may dominate the whole impact, depending primarily on the friction coefficient and velocity of the body. As mentioned, critical condition for the phase of the impact is whether tangential force is less than μF_3, since this condition determines if the body initially sticks or slips.

For the contact point to stick at the beginning of the impact, tangential force must be smaller than the limiting frictional force, that occurs during the slip, such that

$$F_1(0) < \mu F_3(0) \tag{3.52}$$

At the very begining of the impact, $t = \epsilon$, where $\epsilon \ll \omega_o^{-1}\pi/2$, displacement-velocity relation can be expressed as

$$u_1(\epsilon) = \dot{x}(0)\epsilon$$

$$u_3(\epsilon) = \dot{z}(0)\epsilon$$

and the forces are

$$F_1(\epsilon) = -k_1\dot{x}(0)\epsilon$$

$$F_3(\epsilon) = -k_3\dot{x}(0)\epsilon$$

from Equation (3.52) We can have the limit to incidence angle for initial stick

$$\left|\frac{\dot{x}(0)}{\dot{z}(0)}\right| < \mu\frac{k_3}{k_1} \tag{3.53}$$

3.3.1.1.7 Initially Sticking Case If Equation (3.53) is satisfied, the contact point sticks to the surface, hence Equation (3.47) can be solved to yield u_1, u_3, $\dot{u}_1$ and $\dot{u}_3$, from which the motion of the body (and forces) can be found while sticking.

Depending on the modal frequencies that are found from the eigenvalues of the system, sliding may follow sticking, which may then be followed by a reversal. An example of an initially sticking impact is observed with free impact of a sphere. A representative plot is given in Figure 3.4 and more detail about the impact of a sphere will be presented in the following section.

Cases when the sticking phase dominates the whole impact, referred here as gross sticking, is encountered in a planar pendulum, which will be analysed in detail in the following chapter.

3.3.1.1.8 Initially Sliding Case If Equation (3.53) is not satisfied, the massless contact particle slides on the surface, and Equation (3.49) is used. Analytical solution of the differential equation (3.49) can be obtained in terms of u_3 and $\dot{u}_3$ such that:

$$u_3 = \frac{\dot{z}(0)}{\left(a_{33} - a_{31}\mu\hat{s}\right)^{1/2}\omega_o} \sin\left[\left(a_{33} - a_{31}\mu\hat{s}\right)^{1/2}\omega_o t\right] \tag{3.54}$$

where $\omega_o = \sqrt{k_3/m}$. Differentiating (3.54) once gives

$$\dot{u}_3 = \dot{z}(0)\cos\left[\left(a_{33} - a_{31}\mu\hat{s}\right)^{1/2}\omega_o t\right] \tag{3.55}$$

u_1 and $\dot{u}_1$ were related to u_3 and $\dot{u}_3$ respectively, through (3.50) and (3.51) and using Equation (3.48), such that:

$$u_1 = -\frac{k_3}{k_1}\mu\hat{s}\frac{\dot{z}(0)}{\left(a_{33} - a_{31}\mu\hat{s}\right)^{1/2}\omega_o} \sin\left[\left(a_{33} - a_{31}\mu\hat{s}\right)^{1/2}\omega_o t\right] \tag{3.56}$$

$$\dot{u}_1 = -\frac{k_3}{k_1}\mu\hat{s}v_3(0)\cos\left[\left(a_{33} - a_{31}\mu\hat{s}\right)^{1/2}\omega_o t\right] \tag{3.57}$$

Transition from sliding to sticking is found from sliding velocity, $s = \dot{x} - \dot{u}_1$, hence $\dot{x}$ must be calculated. There are two approaches to calculate normal and tangential velocities of the pendulum: (i) Forces can be used to calculate

accelerations, and then accelerations can be integrated to get the velocities, or (ii) forces are used to calculate the impulses by integration and these are used to calculate the velocities, such that

$$\ddot{x} = \frac{d^2x}{dt^2} = (a_{11}F_1 + a_{13}F_3) \tag{3.58}$$

$$\ddot{z} = \frac{d^2z}{dt^2} = (a_{31}F_1 + a_{33}F_3) \tag{3.59}$$

or

$$\dot{x} = (a_{11}P_1 + a_{13}P_3) \tag{3.60}$$

$$\dot{z} = (a_{31}P_1 + a_{33}P_3) \tag{3.61}$$

where

$$P_i = \int F_i dt \qquad i = 1, 3 \tag{3.62}$$

Same results are obtained with both methods and the results are presented in Figure 3.1 for $\mu = 0.5$ and $\theta = 50^o$. In Figure 3.1 solid line represents the result obtained via integration of Equations (3.58) and (3.59)and the circles show the result obtained with Equations (3.60)-(3.62).

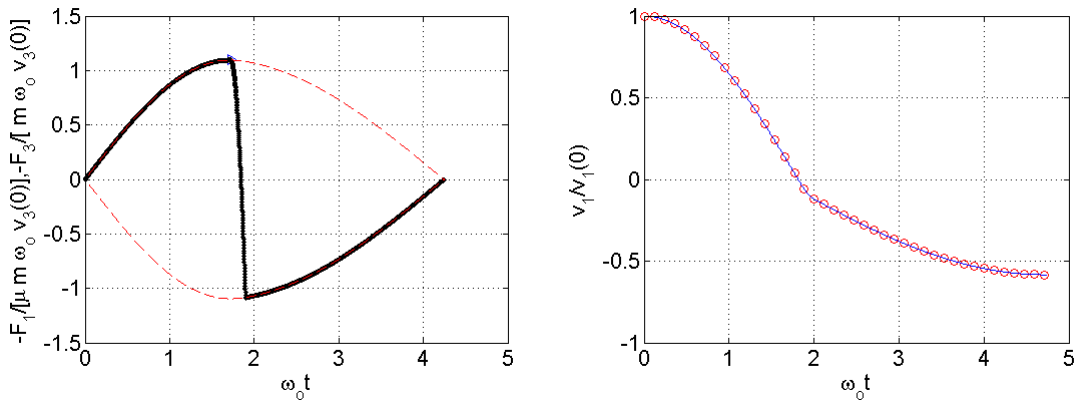

Figure 3.1: Comparison of the different methods used to calculate velocity

In order to obtain an analytical solution for $\dot{x}$ to calculate s, Equation (3.42) is used

$$\frac{d^2x}{dt^2} = (a_{11}F_1 + a_{13}F_3)$$

and using Equation (3.48)

$$\frac{d^2x}{dt^2} = (-a_{11}\mu\hat{s}F_3 + a_{13}F_3)$$

integrating both sides of the above equation gives

$$\dot{x} = (-a_{11}\mu\hat{s} + a_{13}) \int_0^{t_{lt}} F_3 dt + C_1 \tag{3.63}$$

Since at $t = 0$, $P_3(0) = 0$, $C_1 = \dot{x}(0)$ and using Equation (3.54)

$$F_3 = -k_3 u_3 = -k_3 \frac{\dot{z}(0)}{(a_{33} - a_{31}\mu\hat{s})^{1/2}\,\omega_o} \sin\left[(a_{33} - a_{31}\mu\hat{s})^{1/2}\,\omega_o t\right]$$

integration of F_3 gives

$$P_3 = \int F_3 dt = k_3 \frac{\dot{z}(0)}{(a_{33} - a_{31}\mu\hat{s})\,\omega_o^2} \cos\left[(a_{33} - a_{31}\mu\hat{s})^{1/2}\,\omega_o t\right] + C_2 \tag{3.64}$$

with $P_3(0) = 0$

$$C_2 = -k_3 \frac{\dot{z}(0)}{(a_{33} - a_{31}\mu\hat{s})\,\omega_o^2} \tag{3.65}$$

As described earlier, sliding may stop at time t_{lt}, if $s = 0$ condition is met and equation for sliding velocity can be written explicitly

$$\begin{aligned} &s(t) = \dot{x}(0) + \\ &m^{-1}\,(-a_{11}\mu\hat{s} + a_{13}) \left\{ k_3 \frac{\dot{z}(0)}{(a_{33} - a_{31}\mu\hat{s})\,\omega_o^2} \cos\left[(a_{33} - a_{31}\mu\hat{s})^{1/2}\,\omega_o t\right] - k_3 \frac{\dot{z}(0)}{(a_{33} - a_{31}\mu\hat{s})\,\omega_o^2} \right\} \\ &+\mu\hat{s}\frac{k_3}{k_1}\dot{z}(0) \cos\left[(a_{33} - a_{31}\mu\hat{s})^{1/2}\,\omega_o t\right] \end{aligned}$$

$$\begin{aligned} s(t) = \dot{x}(0) + \frac{(a_{13} - a_{11}\mu\hat{s})}{(a_{33} - a_{31}\mu\hat{s})}\dot{z}(0) \left\{ \cos\left[(a_{33} - a_{31}\mu\hat{s})^{1/2}\,\omega_o t\right] - 1 \right\} \\ + \mu\hat{s}\frac{k_3}{k_1}\dot{z}(0) \cos\left[(a_{33} - a_{31}\mu\hat{s})^{1/2}\,\omega_o t\right] \end{aligned} \tag{3.66}$$

and with $s(t_{lt}) = 0$, t_{lt} can be calculated

$$t_{lt} = \frac{1}{(a_{33} - a_{31}\mu\hat{s})^{1/2}\,\omega_o} \cos^{-1}\left\{ \frac{\dot{x}(0)/\dot{z}(0) + (a_{11}\mu\hat{s} - a_{13})\,/\,(a_{33} - a_{31}\mu\hat{s})}{\mu\hat{s}\frac{k_3}{k_1} + (a_{11}\hat{s}\mu - a_{13})/(a_{33} - a_{13}\hat{s}\mu)} \right\} \tag{3.67}$$

If t_{lt} is larger than the duration of contact, t_f, it means there is *gross slip*, i.e. body slides during the entire duration of impact, or if $t_{lt} < t_f$ sticking begins at t_{lt} and Equation (3.47) should be solved with the initial conditions $u_1(t_{lt})$, $u_3(t_{lt})$,

$\dot{u}_1(t_{lt})$ and $\dot{u}_3(t_{lt})$. Initially sliding impact followed by sticking, usually causes reversal in tangential force. Then at t_{tl} sliding may initiate again if Equation (3.48) is satisfied. After $t = t_{tl}$, Equation (3.49) is solved again with proper initial conditions. Figure 4.6 presents an example of this type of impact for a pendulum.

Possible collision conditions for an frictional oblique impact are summarized in Figure 3.2.

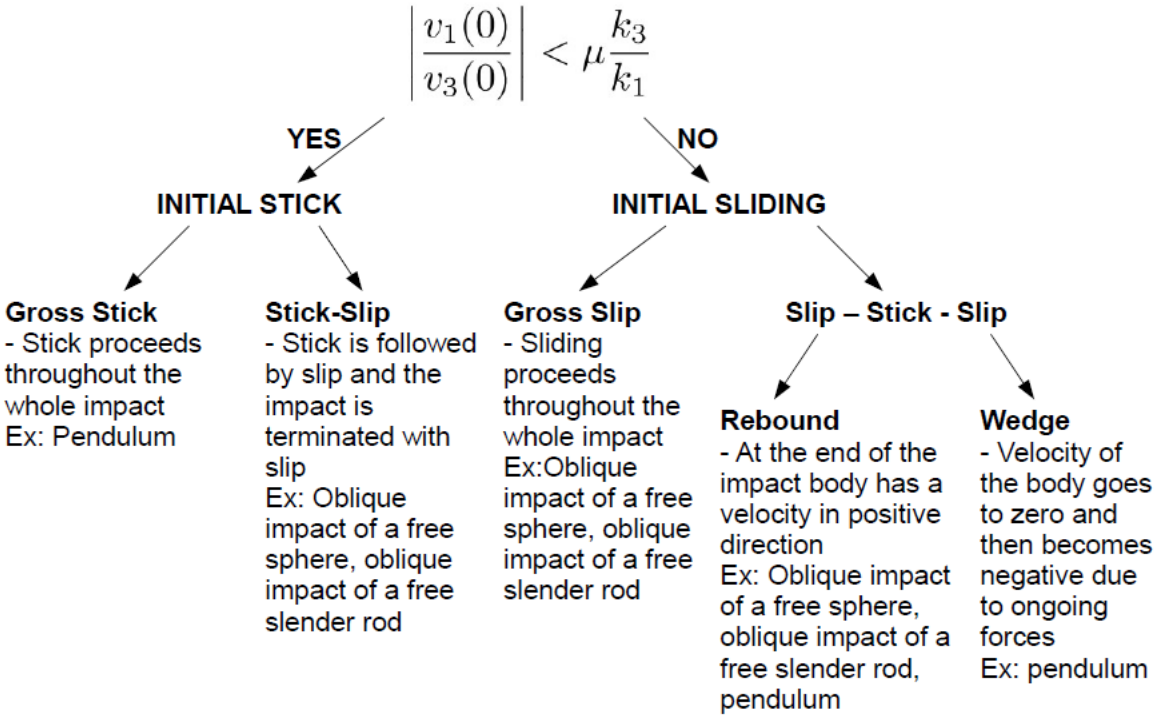

Figure 3.2: Summary of conditions in an oblique impact

3.3.1.2 Examples of Impact with Compliant Elements Model

Concept of compliant elements was explained in general in the previous section. Now, two examples using the method will be given: (i) impact of a free sphere on a frictional massive plane, (ii) impact of an oblique slender rod on a frictional massive plane, to illustrate the behavior of the colliding bodies with simple cases.

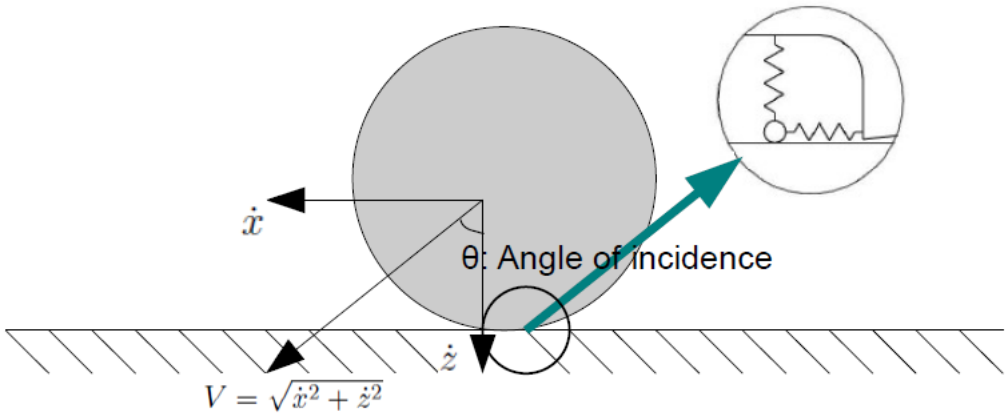

Figure 3.3: Schematic representation of impact of a sphere with compliant elements

3.3.1.2.1 Impact of a Sphere on a Frictional Massive Plane Stronge's work on impact of a sphere on a massive surface [3] is reviewed here as it demonstrates the results developed by Maw et al. [4].

In a collinear impact of a sphere, normal and tangential components of the system are decoupled. Hence sets of differential equations given in the previous section can be solved analytically. Elements of inertia tensor can be found using matrix **B** in Equation (3.36) and then can be used in Equation (3.41) given in [3]. The inertia tensor for a sphere:

$$J = \begin{bmatrix} \frac{2}{5}mR^2 & 0 & 0 \\ 0 & \frac{2}{5}mR^2 & 0 \\ 0 & 0 & \frac{2}{5}mR^2 \end{bmatrix} \tag{3.68}$$

with the inverse of the matrix:

$$J^{-1} = \begin{bmatrix} \frac{5}{2mR^2} & 0 & 0 \\ 0 & \frac{5}{2mR^2} & 0 \\ 0 & 0 & \frac{5}{2mR^2} \end{bmatrix} \tag{3.69}$$

where elements of the position vector used in **B** matrix are: $x = 0$, $y = 0$ and

$z = -R$. Replacing these in the matrix given in Equation (3.36) yields:

$$\mathbf{B} = \begin{bmatrix} m^{-1}\frac{7}{2} & 0 & 0 \\ 0 & m^{-1}\frac{7}{2} & 0 \\ 0 & 0 & m^{-1} \end{bmatrix} \tag{3.70}$$

Reducing the above matrix for 3D, to a planar motion on the plane of $\mathbf{n_1}$ and $\mathbf{n_3}$ gives:

$$\mathbf{B} = \begin{bmatrix} a_{11} & a_{13} \\ a_{31} & a_{33} \end{bmatrix} = \begin{bmatrix} m^{-1}\frac{7}{2} & 0 \\ 0 & m^{-1} \end{bmatrix} \tag{3.71}$$

Modal frequencies, ω, Ω, can be found from the eigenvalues of the system, see Equation (3.47) such that

$$\Omega, \omega = \frac{1}{2}k_1 a_{11} + \frac{1}{2}k_3 a_{33} \pm \frac{1}{2m}\left[\left((k_1 a_{11} - k_3 a_{33})^2 + 4k_3 a_{31}^2 k_1\right)^{1/2}\right] \tag{3.72}$$

Since the compliant elements are assumed to be decoupled during stick, both elements undergo independent simple harmonic motion with the modal frequencies, ω and Ω. Schematic representation of the compliance elements are presented in Figure 3.3.

Normal Components of Velocity and Force

Using Equation (3.47) we can obtain displacement, u_3, relative velocity, v_3, force, F_3, and impulse, P_3, in the normal direction, such that:

$$u_3(t) = \frac{\dot{z}(0)}{\Omega}\sin\Omega t \tag{3.73}$$

$$\dot{z}(t) = \dot{z}(0)\cos\Omega t \tag{3.74}$$

$$F_3(t) = -a_{33}^{-1}\Omega\dot{z}(0)\sin\Omega t \tag{3.75}$$

$$P_3(t) = -a_{33}^{-1}\dot{z}(0)\left(1 - \cos\Omega t\right) \tag{3.76}$$

Tangential Velocity and Force

Sliding or sticking may occur during collision, depending on the impact configuration, ratio of the normal and tangential stiffnesses, and coefficient of friction.

There are three possibilities for a planar impact [3]; (i) if the angle of incidence is small and friction coefficient is high enough, the body initially sticks and then sliding begins, if this condition is not met, then the body slides initially and then there are two possibilities; (ii) sliding continues throughout the impact or (iii) sliding is followed by stick and then sliding starts near the end of the collision period.

As discussed, during stick tangential component of the displacement, force and velocity undergo a simple harmonic motion. If the body sticks at $t = \tau$, from Equation (3.47) one can obtain

$$u_1(t) = u_1(\tau)\cos\omega(t-\tau) + \omega^{-1}\dot{x}(\tau)\sin\omega(t-\tau) \tag{3.77}$$

$$\dot{x}(t) = -\omega u_1(\tau)\sin\omega(t-\tau) + \dot{x}(\tau)\cos\omega(t-\tau) \tag{3.78}$$

$$F_1(t) = -k_1 u_1(\tau)\cos\omega(t-\tau) - k_1\omega^{-1}\dot{x}(\tau)\sin\omega(t-\tau) \tag{3.79}$$

Initially Sticking Case

If condition in Equation (3.53) is satisfied, it means the body sticks at the beginning of the impact and from Equations (3.77)-(3.79), tangential components during sticking (from $0 < t < t_\sigma$) can be described as

$$u_1(t) = \omega^{-1}\dot{x}(0)\sin\omega(t) \quad t < t_\sigma \tag{3.80}$$

$$\dot{u}_1(t) = \dot{x}(t) = \dot{x}(0)\cos\omega(t) \quad t < t_\sigma \tag{3.81}$$

$$F_1(t) = -k_1\omega^{-1}\dot{x}(0)\sin\omega(t) \quad t < t_\sigma \tag{3.82}$$

Impulse between $t = 0$ *to* t_σ can be calculated using tangential force, such that

$$P_1(t) = \int F_1 dt$$

$$P_1(t) = k_1\dot{x}(0)[\cos\omega t - 1] \quad t < t_\sigma \tag{3.83}$$

Sliding starts at $t = t_\sigma$. During sliding, $F_1 = -\mu\hat{s}F_3$, using Equations (3.50) and (3.73)

$$u_1(t) = -\mu\hat{s}\frac{\dot{z}(0)}{\Omega}\sin\Omega t\frac{k_3}{k_1} \quad t \geq t_\sigma \tag{3.84}$$

$$F_1 = -\mu \hat{s} F_3 = \mu \hat{s} a_{33}^{-1} \Omega \dot{z}(0) \sin \Omega t \quad t \geq t_\sigma \tag{3.85}$$

between t_σ and t_f

$$P_1 = \int F_1 dt = \int \mu \hat{s} a_{33}^{-1} \Omega \dot{z}(0) \sin \Omega t \, dt \tag{3.86}$$

$$P_1(t) = -a_{33}^{-1} \hat{s} \mu \dot{z}(0) \cos \Omega t + C \tag{3.87}$$

$$P_1(t_\sigma) = -a_{33}^{-1} \hat{s} \mu \dot{z}(0) \cos \Omega t_1 + C \rightarrow C = a_{33}^{-1} \hat{s} \mu \dot{z}(0) \cos \Omega t_1 + P_1(t_\sigma) \tag{3.88}$$

$$P_1(t) = -a_{33}^{-1} \hat{s} \mu \dot{z}(0) \cos \Omega t + \mu a_{33}^{-1} \hat{s} \dot{z}(0) \cos \Omega t_\sigma + P_1(t_\sigma) \quad t_\sigma < t < t_f \tag{3.89}$$

For the tangential velocity

$$d\dot{x} = a_{11} dP_1 \tag{3.90}$$

$$d\dot{x} = a_{11}(-\mu \hat{s} P_3) \tag{3.91}$$

integrating Equation (3.91) for any time, t_x, between t_σ and t_f produces

$$\int_{t_1}^{t_x} d\dot{x} = -\int_{t_\sigma}^{t_x} a_{11} \mu \hat{s} P_3 \tag{3.92}$$

and with $\hat{s} = +1$, the tangential velocity becomes

$$\dot{x}(t_x) = \dot{x}(t_\sigma) - \frac{\mu}{a_{11}} [P_3(t_x) - P_3(t_\sigma)] \quad t_\sigma < t < t_f \tag{3.93}$$

An example of such an impact is presented in Figure 3.4. The plot on the left-hand side shows the normalized tangential velocity (solid line) and the normalized normal force envelope (dashed line) and on the right-hand side velocity plots are presented. As seen from sliding velocity, s, plot, initally relative velocity is zero at the contact point, indicating sticking. The body compresses the tangential spring element transferring its energy and at the time where $\dot{u}_1$ is zero, maximum compression on the tangential compliant element is reached. Then, the compression in the spring decreases at the time where F_1 is zero, and elongation of the element begins. After this point tangential force reversal occurs and sliding starts when the tangential force is equal to μF_3.

Initially Sliding Case

If the inequality in Equation (3.53) is not met, the body initially slides. In this case, there are two possibilities: (i) sliding may continue throughout the

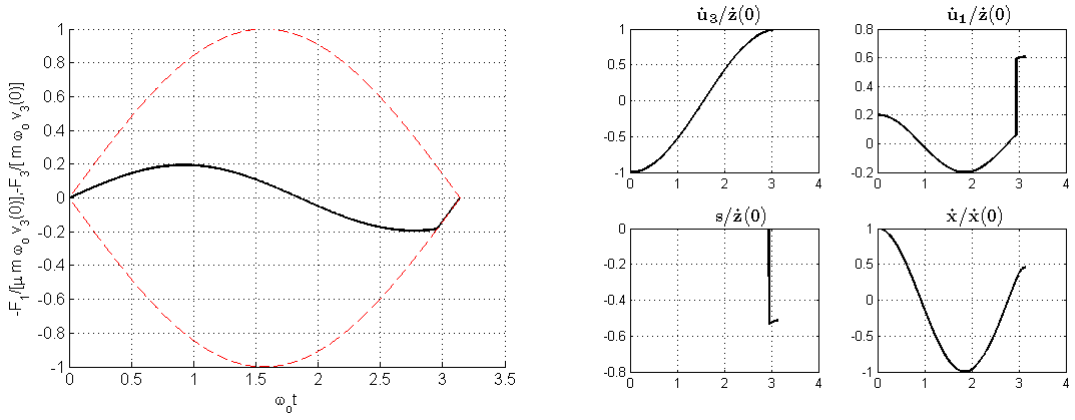

Figure 3.4: Impact of a sphere with $\mu = 0.5$, $\dot{x}(0)/\dot{z}(0) = 0.2$, $k_3/k_1 = 1.21$

collision or (ii) it terminates at $t = t_{lt}$ and sticking begins. If sticking occurs after initial sliding, generally sliding follows it at some time close to end of the impact. Sliding to sticking condition can be found using (3.52).

During the collision, normal components remain the same due to the fact that the system is uncoupled, and Equations (3.73-3.76) can be used. For the tangential component, the equalities can be calculated using Equation (3.48) with Equation (3.75)

$$F_1 = \mu \hat{s} a_{33}^{-1} \Omega \dot{z}(0) \sin \Omega t \tag{3.94}$$

again with Equation (3.48) and Equations (3.44,3.45)

$$u_1 = -\mu \hat{s} \frac{k_3}{k_1} \dot{z}(0) \Omega^{-1} \sin \Omega t \tag{3.95}$$

differentiating once

$$\dot{u}_1 = -\mu \hat{s} \frac{k_3}{k_1} \dot{z}(0) \cos \Omega t \tag{3.96}$$

impulse bewteen $t = 0$ and t_{lt}

$$P_1 = \int_0^{t_{lt}} F_1 dt = \int_0^{t_{lt}} \mu \hat{s} a_{33}^{-1} \Omega \dot{z}(0) \sin \Omega t \, dt$$

$$P_1 - \mu \hat{s} a_{33}^{-1} \dot{z}(0) \cos \Omega t + C$$

$$P_1(0) = 0 \rightarrow C = \mu \hat{s} a_{33}^{-1} \dot{z}(0)$$

$$P_1 = -\mu \hat{s} a_{33}^{-1} \dot{z}(0) \cos \Omega t + \mu \hat{s} a_{33}^{-1} \dot{z}(0) \qquad 0 < t < t_{lt} \tag{3.97}$$

for the tangential velocity of the body at time $t = t_x$ between 0 and t_{lt}

$$d\dot{x} = a_{11} dP_1$$

$$\dot{x}(t_x) = \dot{x}(0) + a_{11} P_1(t_x) \tag{3.98}$$

At $t = t_{lt}$ sticking may begin. During sticking, again Equations (3.77) to (3.79) can be used to calculate u_1, v_1 and F_1. Differentiating Equation (3.77) gives $\dot{u}_1$ and integrating Equation (3.79) gives P_1 between t_{lt} and t_{tl}, where t_{tl} is the time when sliding initiates again and can be found from the time where $|F_1| = \mu F_3$.

For the final sliding phase, Equations (3.94-3.96) are used. For the tangential impulse at $t = t_x$, where t_x is any time between $t = t_{lt}$ and $t = t_{tl}$, again integration is needed such that

$$P_1 = \int_{t_{lt}}^{t_x} F_1 dt$$

$$P_1 = \int_{t_{lt}}^{t_x} \mu \hat{s} a_{33}^{-1} \Omega \dot{z}(0) \sin \Omega t \, dt$$

$$P_1 = -\mu \hat{s} a_{33}^{-1} \dot{z}(0) \cos \Omega t + C_3$$

at $t = t_{tl}$, knowing that $P(t_{tl})$ was calculated by the calculations of sticking phase

$$P_1(t_{tl}) = -\mu \hat{s} a_{33}^{-1} \dot{z}(0) \cos \Omega t + C_3 \rightarrow C_3 = \mu \hat{s} a_{33}^{-1} \dot{z}(0) \cos \Omega t_{tl} + P_1(t_{tl})$$

$$P_1(t) = -\mu \hat{s} a_{33}^{-1} \dot{z}(0) \cos \Omega t + \mu \hat{s} a_{33}^{-1} \dot{z}(0) \cos \Omega t_{tl} + P_1(t_{tl}) \tag{3.99}$$

and tangetial velocity at $t_{tl} < t_x < t_f$

$$\dot{x}(t_x) = a_{11} \left[P_1(t_x) - P_1(t_{tl}) \right] + \dot{x}(t_{tl}) \tag{3.100}$$

Figure 3.5 represents impact of a sphere that is initially in sliding phase. Sliding continues until $t = t_{lt}$ where sliding velocity, s, is zero. During sticking tangential force reverses its direction and the spring element starts to elongate.

At $t = t_{tl}$ sliding starts again in the positive direction (note that the direction of motion can be observed in $s/\dot{z}(0)$ plot where $\dot{z}(0) < 0$) and continues until the end of the impact.

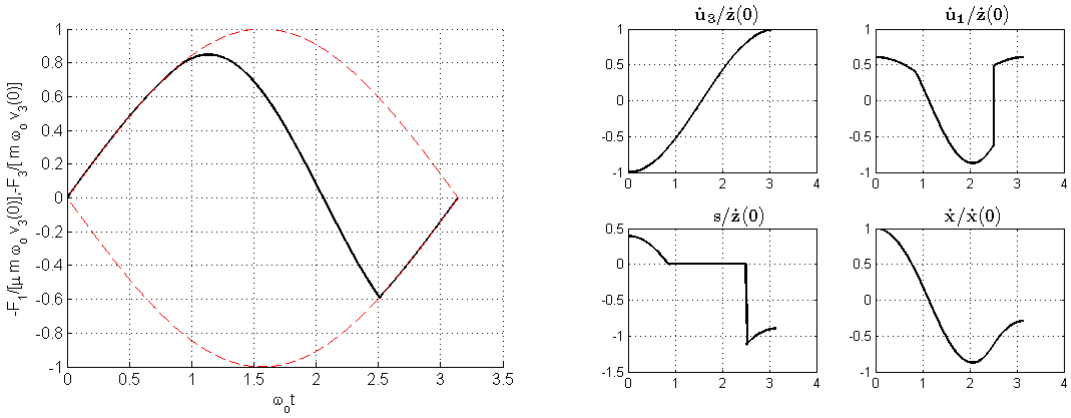

Figure 3.5: Impact of a sphere with $\mu = 0.5$, $\dot{x}(0)/\dot{z}(0) = 1$, $k_3/k_1 = 1.21$

To show the effect of tangential compliance compared with the classical theory, normalized final tangential velocities of an impacting sphere with respect to normalized initial tangential velocity are presented. At small angles of incidence, signs of initial and final tangential velocities are the same. However, at intermediate angles of incidence, reversal of direction can be seen clearly, which is the main difference between negligible tangential compliance assumption and the model with tangential compliance. Stronge [3] compares his results with those of Maw et al. [4] and points out that compliant elements method gives very similar result to Maw et al. and without need for excessive computational time, thus supporting the use of compliant elements in constrained impact problem treated in this thesis.

3.3.1.2.2 Impact of an Oblique Slender Rod on a Frictional Surface

In this section study of Stronge et. al. [30] is reviewed to illustrate an eccentric free impact with compliant elements at the contact.

As a second example using compliant elements in impact, a slender rod with a uniformly distributed mass, m, with an inclination to vertical plane, θ, (see Figure 3.7) colliding on a massive plate is presented to illustrate an eccentric free

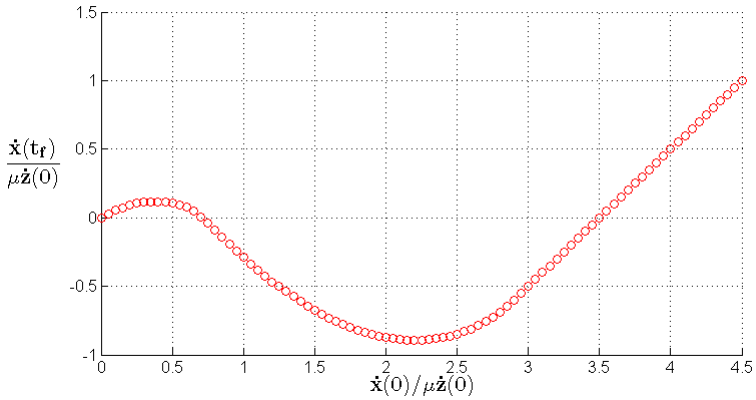

Figure 3.6: Final tangential velocities for changing initial tangential velocities for oblique impact of a sphere

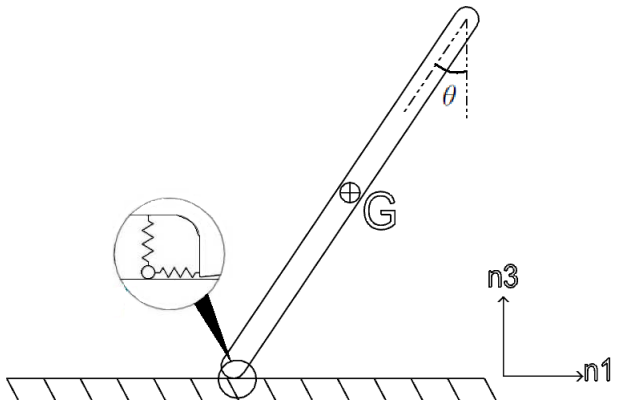

Figure 3.7: Schematic representation of an impacting slender rod with lumped parameter model

impact. The equations describing its behavior during impact are [30]:

$$a_{11} = m^{-1}\left(1 + 3\cos^2\theta\right) \tag{3.101}$$

$$a_{13} = a_{31} = m^{-1}\left(3\sin\theta\cos\theta\right) \tag{3.102}$$

$$a_{33} = m^{-1}\left(1 + 3\sin^2\theta\right) \tag{3.103}$$

Since normal and tangential components of the system are coupled, related differential equations can not be solved analytically. For numerical solutions, the equations to be solved are selected according to whether the contact point is in initially sticking or initially sliding phase, using Equation (3.53).

Initially Sticking Case

If the inequality in Equation (3.53) is satisfied, contact point initially sticks, i.e. $\dot{u_1} = \dot{x}$ and Equation (3.47) is solved numerically for sticking condition. Solution of the set of differential equations in Equation (3.47), with the initial conditions $u_1 = u_3 = 0$, $\dot{u}_1 = \dot{x}(0)$ and $\dot{u}_3 = \dot{z}(0)$, gives displacements and velocities of the spring elements in tangential and normal directions. When Equation (3.48) is satisfied, i.e. when tangential force overcomes friction force, sliding starts at t_σ. Then the equations that are valid for sliding (Equation (3.49) for u_3 and $\dot{u}_3$ with initial conditions $u_3(t_\sigma)$ and $\dot{u}_3(t_\sigma)$ and Equations (3.50) and (3.51) for u_1 and $\dot{u}_1$) can be used. An example of such a collision is presented in Figure 3.8. On the left-hand side of Figure 3.8, as before, the solid line shows the normalized tangential force and dashed lines show the normalized normal force envelope and on the right-hand side, rates of displacements of spring elements, sliding velocity and tangential velocity of the body are presented, respectively. From Figure 3.8 it can be seen that up to time t_σ tangential force is less than the normalized normal force, i.e. friction force, and hence sticking is observed. For this example, initial tangential velocity is in positive direction and as a result, the tangential force is in opposite (negative) direction. Until the normalized time, $\omega_o t$ is about 0.7, the energy of the system is transferred to the springs by compressing them. When the compression (i.e. the tangential force) becomes maximum, all the energy is already transferred to the compliant elements and hence tangential velocity of the spring element vanishes (see $\dot{u}_1$ plot). After $\dot{u}_1$ vanishes, compression in

the tangential spring element decreases and the energy in the spring elements is transferred back to the body. After u_1 vanishes reversal of the tangential force occurs. After reversal, the contact point is still attached to the surface and the spring element in the tangential direction is elongated. At t_σ tangential force is equal to the μF_3 and sliding starts.

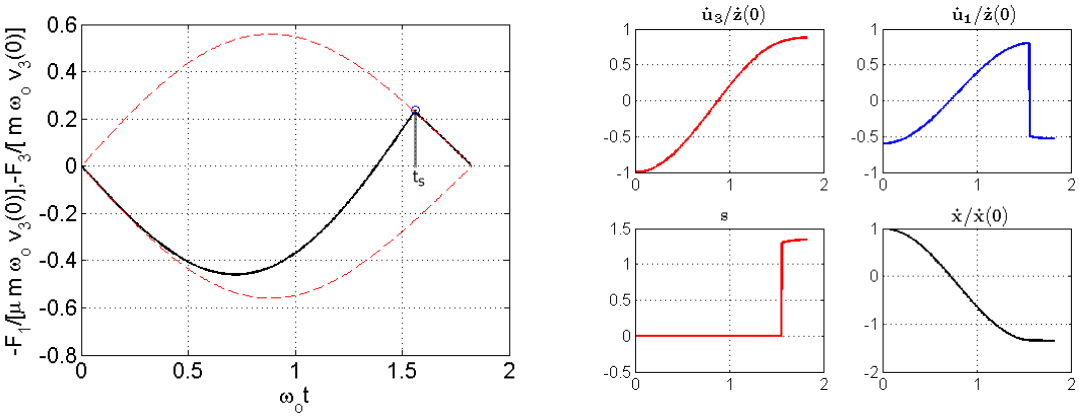

Figure 3.8: Oblique impact of a rod with $\theta = 45^o$, $\mu = 0.6$, $k_3/k_1 = 1.21$, $\dot{x}(0)/\dot{z}(0) = -0.6$

Initially Sliding Case

If the inequality in Equation (3.53) is not satisfied, impact initiates with sliding. Solving Equation (3.49) with $u_3(0)$ and $\dot{u}_3(0)$ numerically, gives the normal component of spring element's motion. Then, using Equations (3.50) and (3.51) u_1 and $\dot{u}_1$ can be found. At $t = t_{lt}$ sliding terminates and sticking starts and this can be found by using Equation (3.67). Note that Equation (3.67) can be used to find the time when sliding velocity, s, is zero. Then sticking begins and solving Equation (3.47) with the initial conditions $u_1(t_{lt})$, $u_3(t_{lt})$, $\dot{u}_1(t_{lt})$ and $\dot{u}_3(t_{lt})$ numerically, gives the kinematic variables of the system. Using tangential and normal displacements, corresponding force components are calculated (Equations (3.44) and (3.45)) and when tangential force becomes equal to the friction force (μF_3), sliding starts again at t_{tl}. Again, Equations (3.49), (3.50), (3.51) are used to find related displacements. Note that there is a possibility that during entire impact, sliding takes place (*gross slip*) depending on the angle of incidence. This can be caught mathematically if $t_{lt} > t_f$, where t_f is the time when the impact ends.

In Figure 3.9, an example for an initially sliding rod is presented. Up to $t = t_{lt}$, contact point slides with a decreasing sliding velocity by compressing the tangential spring element, when $t = t_{lt}$ sliding velocity becomes zero and sticking begins. After this point compression in the tangential spring decreases and becomes zero after some time, this can be seen in the left-hand side plot where tangential force becomes zero. However sticking still continues and the spring element is elongated. At $t = t_{tl}$ tangential force reaches μF_3, and sliding starts and continues until the end of the impact period.

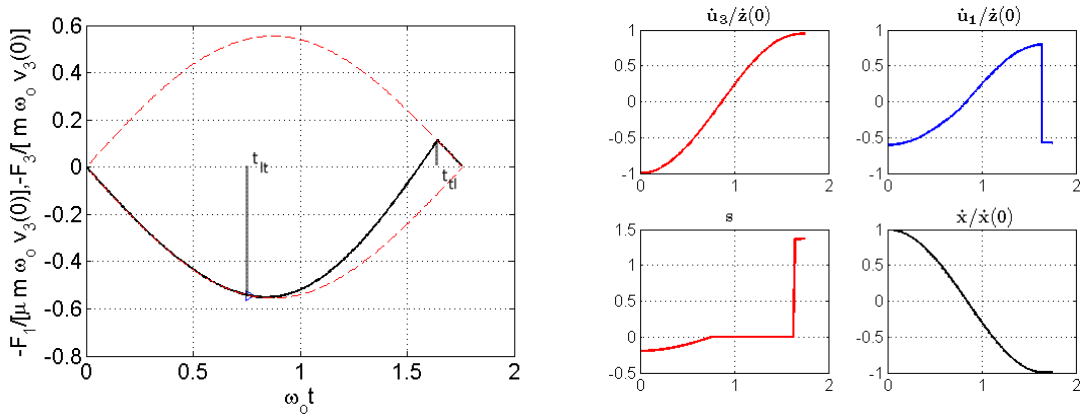

Figure 3.9: Oblique impact of a rod with $\theta = 45^o$, $\mu = 0.6$, $k_3/k_1 = 1.21$, $\dot{x}(0)/\dot{z}(0) = -0.8$

Chapter 4

Constrained Collisions

This chapter treats collision of objects that are constrained. General equations derived for free impacts are modified and equations for constrained impact are obtained. These relations are used to model contact with compliant elements.

In multi-body systems, the motion of the bodies can be hindered by physical connections decreasing the degree of freedom of the system. The motion of such hindered systems are called *constrained motions* and form the basis of mechanisms. Dynamics of these systems differ from the dynamics of the free bodies in the sense that constraints are imposed on the related equations to solve for the response of the system.

Impact of a constrained body is analysed in a similar manner with the collision of free bodies. However, frictional impacts, non-rigid connections, eccentricity of the impact, locking of the system etc. require further analysis compared to free impact of bodies.

A pendulum represents a very basic example of a constrained motion, which consists of a mass connected with a link to a point about which it can pivot. Only rotational motion is allowed and degrees of freedom of the system (the axes about which the mass can rotate) depend on the nature of the joint. In the next section, of the thesis basic equations for a simple pendulum having two degrees of

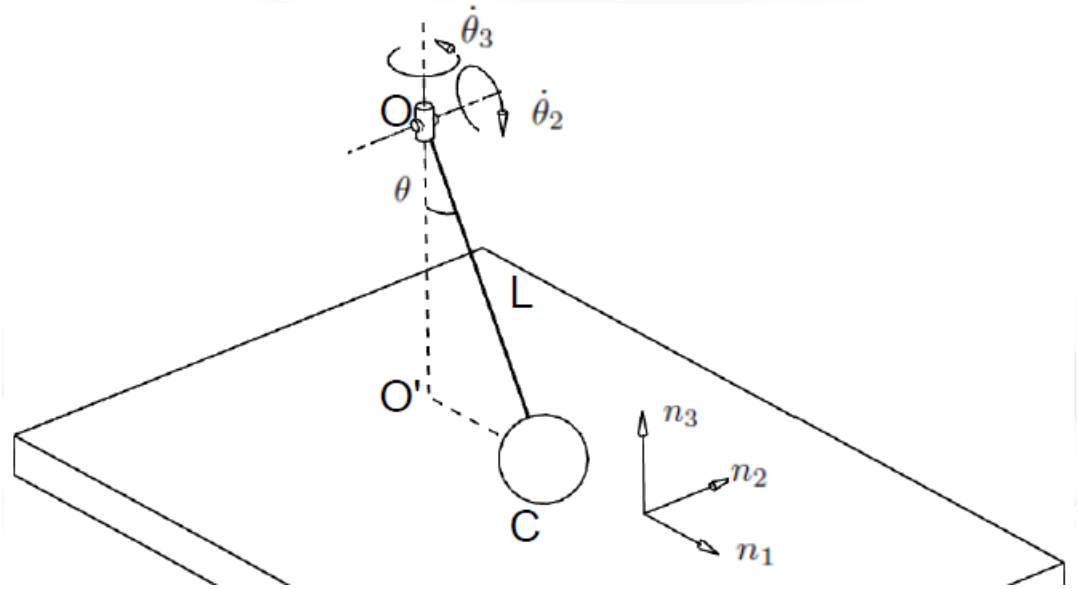

Figure 4.1: Impact of a pendulum with two degrees of freedom

freedom and a physical pendulum having one degree of freedom (planar motion) will be derived with detailed explanations of the system.

4.1 Impact of a 3D Pendulum

As described in Figure 4.1 pendulum is pivoted about point O. The pendulum is able to rotate about $\mathbf{n_2}$ and $\mathbf{n_3}$ axes but rotation about $\mathbf{n_1}$ is hindered. In addition, linear motion of the pendulum in all three axes is hindered. Mass of the sphere at the tip of the pendulum will be denoted by m and the length between points O and C will be shown by L.

General form of the equation for the velocity at the contact point of two free bodies is given in Equation (3.19) as:

$$\mathbf{\Delta V_R} = (\mathbf{\Delta V} - \mathbf{\Delta V'}) + \left(\mathbf{\Delta \dot{\theta}} \times \boldsymbol{\rho} - \mathbf{\Delta \dot{\theta}'} \times \boldsymbol{\rho'}\right)$$

Since pendulum is constrained at point O and only rotation is allowed, $\mathbf{\Delta V} = \mathbf{\Delta V'} = 0$. In addition, the second body is considered here as a stationary rough

half-space, so that the general equation reduces to:

$$\boldsymbol{\Delta V_R} = \boldsymbol{\Delta \dot{\theta}} \times \boldsymbol{\rho_o} \tag{4.1}$$

where $\boldsymbol{\rho_o}$ represents the vector from point O (hinge) to the contact point C.Angular velocity change, $\boldsymbol{\Delta \dot{\theta}}$, of the pendulum due to impact can be obtained from using Equation (3.13):

$$\boldsymbol{J_o \Delta \dot{\theta}} = \boldsymbol{\rho_o} \times \boldsymbol{P} \tag{3.13}$$

Multiplying both sides of the above equation with inverse of the inertia tensor, $\mathbf{J_o}^{-1}$, gives the angular velocities, which can be used to find the components of relative velocity at the contact point.

Elements of the inertia tensor about point O are calculated using the parallel axis theoem:

$$J_o = J_{cm} + md^2$$

For the derivation of 3D impulse-momentum relations, a simple pendulum with a point mass, m, rotating about point O, is considered. For a point mass, moment of inertia about the center of mass is zero, i.e. $J_{ii} = 0$ and $J_{ij} = 0$.

$$J_{11} = 0 + m\left(y_o^2 + z_o^2\right)$$

$$J_{22} = 0 + m\left(x_o^2 + z_o^2\right)$$

$$J_{33} = 0 + m\left(x_o^2 + y_o^2\right)$$

$$J_{12} = 0 - mx_o y_o = J_{21}$$

$$J_{13} = 0 - mx_o z_o = J_{31}$$

$$J_{23} = 0 - my_o z_o = J_{32}$$

where x_o, y_o and z_o represent the positions from point O to C in directions $\mathbf{n_1}$, $\mathbf{n_2}$ and $\mathbf{n_3}$, respectively. Placing the coordinate system such that $\mathbf{n_1}$ and $\mathbf{n_3}$ plane passes through points O, C and the O' (which is the projection of point O to the impact plane in the plane's normal direction), x_o, y_o and z_o can be expressed as:

$$x_o = L\ \sin\theta$$

$$y_o = 0$$

$$z_o = -L\,\cos\theta$$

which are also the elements of $\boldsymbol{\rho_o}$. As a result, the inertia tensor becomes:

$$\mathbf{J}_o = \begin{bmatrix} mL^2\cos^2\theta & 0 & -mL^2\sin\theta\cos\theta \\ 0 & mL^2 & 0 \\ -mL^2\sin\theta\cos\theta & 0 & mL^2\sin^2\theta \end{bmatrix}$$

In order to solve $\mathbf{J}_o\,\boldsymbol{\Delta\dot{\theta}} = \boldsymbol{\rho_o} \times \mathbf{P}$ for $\boldsymbol{\Delta\dot{\theta}}$, inverse of the $\mathbf{J_o}$ matrix, $\mathbf{J_o}^{-1}$, is needed. However, since $\mathbf{J_o}$ is singular, inverse of the inertia matrix is undefined. Hence, additional constraints are required to relate angular velocity to impulse. As a result, constraints, $\dot{\theta}_1 = 0$ and $\ddot{\theta}_1 = 0$, are imposed on the equations, such that:

$$\mathbf{J_o}\,\boldsymbol{\Delta\dot{\theta}} = \boldsymbol{\rho_o} \times \mathbf{P}$$

$$\begin{bmatrix} J_{11} & 0 & J_{13} \\ 0 & J_{22} & 0 \\ J_{31} & 0 & J_{33} \end{bmatrix} \begin{bmatrix} 0 \\ \Delta\dot{\theta}_2 \\ \Delta\dot{\theta}_3 \end{bmatrix} = \begin{bmatrix} x_o \\ y_o \\ z_o \end{bmatrix} \times \begin{bmatrix} P_1 \\ P_2 \\ P_3 \end{bmatrix}$$

$$\begin{bmatrix} J_{11} & 0 & J_{13} \\ 0 & J_{22} & 0 \\ J_{31} & 0 & J_{33} \end{bmatrix} \begin{bmatrix} 0 \\ \Delta\dot{\theta}_2 \\ \Delta\dot{\theta}_3 \end{bmatrix} = \begin{bmatrix} y_o\,P_3 - z_o\,P_2 \\ z_o\,P_1 - x_o\,P_3 \\ x_o\,P_2 - y_o\,P_1 \end{bmatrix}$$

$$J_{13}\,\Delta\dot{\theta}_3 = y_o\,P_3 - z_o\,P_2 \rightarrow \Delta\dot{\theta}_3 = \frac{1}{J_{13}}\,(y_o\,P_3 - z_o\,P_2) \tag{4.2}$$

$$J_{22}\,\Delta\dot{\theta}_2 = z_o\,P_1 - x_o\,P_3 \rightarrow \Delta\dot{\theta}_2 = \frac{1}{J_{22}}\,(z_o\,P_1 - x_o\,P_3) \tag{4.3}$$

$$J_{33}\,\Delta\dot{\theta}_3 = x_o\,P_2 - y_o\,P_1 \rightarrow \Delta\dot{\theta}_3 = \frac{1}{J_{33}}\,(x_o\,P_2 - y_o\,P_1) \tag{4.4}$$

From the differential form of Equation (4.1) $\mathbf{\Delta V_R} = \boldsymbol{\Delta\dot{\theta}} \times \boldsymbol{\rho}$, we have:

$$\begin{bmatrix} \Delta V_1 \\ \Delta V_2 \\ \Delta V_3 \end{bmatrix} = \begin{bmatrix} \Delta\dot{\theta}_1 \\ \Delta\dot{\theta}_2 \\ \Delta\dot{\theta}_3 \end{bmatrix} \times \begin{bmatrix} x_o \\ y_o \\ z_o \end{bmatrix}$$

with $\Delta\dot{\theta}_1 = 0$ and $y_o = 0$:

$$\begin{bmatrix} \Delta V_1 \\ \Delta V_2 \\ \Delta V_3 \end{bmatrix} = \begin{bmatrix} \Delta\dot{\theta}_2\,z_o \\ \Delta\dot{\theta}_3\,x_o \\ -\Delta\dot{\theta}_2\,x_o \end{bmatrix}$$

using Equations (4.3) and (4.4) for $\Delta\dot{\theta}_2$ and $\Delta\dot{\theta}_3$

$$\begin{bmatrix} \Delta V_1 \\ \Delta V_2 \\ \Delta V_3 \end{bmatrix} = \begin{bmatrix} \left[\frac{1}{J_{22}}\left(z_o\, P_1 - x_o\, P_3\right)\right] z_o \\ \left[\frac{1}{J_{33}}\left(x_o\, P_2 - y_o\, P_1\right)\right] x_o \\ -\left[\frac{1}{J_{22}}\left(z_o\, P_1 - x_o\, P_3\right)\right] x_o \end{bmatrix}$$

replacing elements of $\mathbf{J}$ and $\boldsymbol{\rho_o}$

$$\begin{bmatrix} \Delta V_1 \\ \Delta V_2 \\ \Delta V_3 \end{bmatrix} = \frac{1}{m} \begin{bmatrix} \cos^2\theta & 0 & \sin\theta\cos\theta \\ 0 & 1 & 0 \\ \sin\theta\cos\theta & 0 & \sin^2\theta \end{bmatrix} \begin{bmatrix} P_1 \\ P_2 \\ P_3 \end{bmatrix} \tag{4.5}$$

which is in the form that is given in Equation (3.37)

$$\mathbf{\Delta V_R = B\, P}$$

and $\boldsymbol{B}$ is, knowing Equation (3.38)

$$\boldsymbol{B} = \begin{bmatrix} a_{11} & a_{12} & a_{13} \\ a_{21} & a_{22} & a_{23} \\ a_{31} & a_{32} & a_{33} \end{bmatrix} = \frac{1}{m} \begin{bmatrix} \cos^2\theta & 0 & \sin\theta\cos\theta \\ 0 & 1 & 0 \\ \sin\theta\cos\theta & 0 & \sin\theta \end{bmatrix} \tag{4.6}$$

writing Equation (4.5) in open form:

$$m\Delta V_1 = \cos^2\theta P_1 + \cos\theta\sin\theta P_3 \tag{4.7}$$

$$m\Delta V_2 = P_2 \tag{4.8}$$

$$m\Delta V_3 = \sin\theta\cos\theta P_1 + \sin^2\theta P_3 \tag{4.9}$$

4.1.1 Change of Sliding Directions in 3D Impacts

This section presents a summary review of the phenomena of change of sliding directions observed in 3D impacts that analysed in detail in e.g. [40, 56–59].

In 3D impacts with friction there is a possibility of the impact to converge a constant direction line. This behavior can be estimated before solving the non-linear set of differential equations. Starting with the effective mass matrix,$\boldsymbol{B}$, is

described previously in Chapter 3,:

$$\mathbf{B} = \begin{bmatrix} a_{11} & a_{12} & a_{13} \\ a_{21} & a_{22} & a_{23} \\ a_{31} & a_{32} & a_{33} \end{bmatrix}$$

Changes in relative velocity are expressed as a function of differential impulse rather than time since it is known that impulse increases monotonically and remains finite like the time. Then, the equations of motion for changes in relative velocity can be written as:

$$dV_1 = a_{11}\, dP_1 + a_{12}\, dP_2 + a_{13}\, dP_3 \tag{4.10}$$

$$dV_2 = a_{21}\, dP_1 + a_{22}\, dP_2 + a_{23}\, dP_3 \tag{4.11}$$

$$dV_3 = a_{31}\, dP_1 + a_{32}\, dP_2 + a_{33}\, dP_3 \tag{4.12}$$

where the subscripts 1, 2 and 3 represent directions in the coordinate system $\mathbf{n_3}$ being normal to the tangent plane on which the two bodies contact and $\mathbf{n_2}$ and $\mathbf{n_1}$ show the unit vectors in the tangent plane.

Friction between colliding bodies can be represented by Amontons-Coulomb law of sliding friction such that;

$$\sqrt{(dP_1)^2 + (dP_2)^2} < \mu\, dP_3 \qquad if\ V_1^2 + V_2^2 = 0 \tag{4.13}$$

$$dP_1 = -\frac{\mu V_1}{\sqrt{V_1^2 + V_2^2}} dP_3, \qquad dP_2 = -\frac{\mu V_2}{\sqrt{V_1^2 + V_2^2}} dP_3 \qquad if\ V_1^2 + V_2^2 > 0 \tag{4.14}$$

defining sliding speed as

$$s \equiv \sqrt{V1^2 + V_2^2} \tag{4.15}$$

if there is sliding ($s > 0$), the incremental impulsive force due to friction acts in a direction opposite sliding. Using Amontons-Coulomb relations,

$$dV_1/dP_3 = -\mu a_{11} cos\phi - \mu a_{12} sin\phi + a_{13} \tag{4.16}$$

$$dV_2/dP_3 = -\mu a_{21} cos\phi - \mu a_{22} sin\phi + a_{23} \tag{4.17}$$

$$dV_3/dP_3 = -\mu a_{31} cos\phi - \mu a_{32} sin\phi + a_{33} \tag{4.18}$$

where $\phi(P_3)$ is the impulse dependent angle between tangential velocities, i.e. $\tan\phi(P_3) = V_2/V_1$.

If the inertia terms in Equations (4.16) and (4.17) are not proportional to each other, the angle, ϕ, between the tangential velocities vary during sliding. The behavior of this angle is important because it determines the stick-slip behavior.

Knowing the behavior of the tangential velocity is important because the above differential equations must be solved numerically and when the tangential velocity is zero the equations become ill-conditioned (see the $\sqrt{V_1^2 + V_2^2}$ term in the denominator in cosine and sine terms in the equations). As a result, knowing what happens (stick or slip) after $s = 0$ can be determined by analyzing the material (μ, e) and geometrical properties (effective mass matrix, $\mathbf{B}$) of the impacting bodies as described below.

In 3D contact, change of sliding direction are referred as swerve [40] or flow [59]. The flow of the tangential velocity is towards constant direction lines which are classified into two:

1. Isoclinics are constant direction lines that the flow is asymptotically approached if the impact configuration is out of that specific angle

2. Seperatrix is again the constant direction line but it separates two regions where the flows are towards different isoclinic lines below and above this specific angle.

General trend to determine flow characteristics involves expressing the velocities in polar coordinates as a function of normal impulse. Then $d\phi/dp = 0$ gives the constant direction lines (seperatrix or isoclinics) and $ds/dp = 0$ gives the change in flow directions. In addition, by analyzing the fixed points of the differential equations, the behavior between constant direction lines can be found.

The radial component, s, of the sliding speed can be expressed as:

$$s^2 = V_1^2 + V_2^2$$

differentiating both sides with respect to normal impulse, P_3,

$$2\,s\,\frac{ds}{dP_3} = 2\,V_1\,\frac{dV_1}{dP_3} + 2\,V_2\,\frac{dV_2}{dP_3} \tag{4.19}$$

Equations (4.16) and (4.17) are ill-defined when $V_1 = V_2 = 0$ (see sine and cosine terms with the denominator $\sqrt{V_1^2 + V_2^2}$). To avoid this Bhatt and Koechling [58] use "stretching" such that $d\tau = (\mu/\sqrt{V_1^2 + V_2^2})\,dP_3$ and Equations (4.16) and (4.17) become;

$$\frac{dV_1}{d\tau} = \frac{\sqrt{V_1^2 + V_2^2}}{\mu}\left(-\mu a_{11}\frac{V_1}{\sqrt{V_1^2 + V_2^2}} - \mu a_{12}\frac{V_2}{\sqrt{V_1^2 + V_2^2}} + a_{13}\right)$$

$$\frac{dV_1}{d\tau} = -a_{11}V_1 - a_{12}V_2 + \frac{a_{13}}{\mu}\sqrt{V_1^2 + V_2^2} \tag{4.20}$$

similarly

$$\frac{dV_2}{d\tau} = -a_{21}V_1 - a_{22}V_2 + \frac{a_{23}}{\mu}\sqrt{V_1^2 + V_2^2} \tag{4.21}$$

Using Equation (4.19)

$$s\,\frac{ds}{dP_3} = V_1 \underbrace{\frac{dV_1}{dP_3}}_{Equation(4.16)} + V_2 \underbrace{\frac{dV_2}{dP_3}}_{Equation(4.17)}$$

Subtituting

$$s\frac{ds}{dP_3} = V_1\left(-\mu a_{11}\cos\phi - \mu a_{12}\sin\phi + a_{13}\right) + V_2\left(-\mu a_{21}\cos\phi - \mu a_{22}\sin\phi + a_{23}\right)$$

and using stretching again

$$\frac{ds}{d\tau} = s\left[-a_{11}\cos^2\phi - (a_{12} + a_{21})\sin\phi\cos\phi - a_{22}\sin^2\phi + \frac{a_{13}}{\mu}\cos\phi + \frac{a_{23}}{\mu}\sin\phi\right] \tag{4.22}$$

To obtain the change of the angle, $d\phi$, between the two tangential components of velocity can be obtained similarly;

$$\phi = \tan^{-1}(V_2/V_1) \tag{4.23}$$

using

$$\frac{d\left(\tan^{-1}u\right)}{dx} = \frac{1}{1+u^2}\frac{du}{dx}$$

and from quotient rule for derivatives

$$\left(\frac{f}{g}\right)' = \frac{f'g - g'f}{g^2}$$

$$\frac{d\phi}{dP_3} = \frac{d\left(\tan^{-1}\left(V_2/V_1\right)\right)}{dP_3} = \frac{1}{1+\left(V_2/V_1\right)^2}\frac{d\left(V_2/V_1\right)}{dP_3} \tag{4.24}$$

$$\frac{d\phi}{dP_3} = \frac{\not{V}_1^2}{V_1^2+V_2^2}\left[\frac{\left(dV_2/dP_3\right)V_1 - \left(dV_1/dP_3\right)V_2}{\not{V}_1^2}\right] \tag{4.25}$$

From Equations (4.16) and (4.17) dV_2/dP_3 and $dV_1 dP_3$, can be replaced, then

$$\frac{d\phi}{dP_3} = \left[\frac{\left(-\mu a_{21}\cos\phi - \mu a_{22}\sin\phi + a_{23}\right)V_1 - V_2\left(-\mu a_{11}\cos\phi - \mu a_{12}\sin\phi + a_{13}\right)}{V_1^2+V_2^2}\right] \tag{4.26}$$

using stretching $d\tau = \left(\mu/\sqrt{V_1^2+V_2^2}\right)dP_3$

$$\frac{d\phi}{d\tau} = \frac{\sqrt{V_1^2+V_2^2}}{\mu\left(V_1^2+V_2^2\right)}\left[\left(-\mu a_{21}\cos\phi - \mu a_{22}\sin\phi + a_{23}\right)V_1 - V_2\left(-\mu a_{11}\cos\phi - \mu a_{12}\sin\phi + a_{13}\right)\right] \tag{4.27}$$

$$\frac{d\phi}{d\tau} = -a_{21}\cos^2\phi + a_{12}\sin^2\phi + \left(a_{11}-a_{22}\right)\sin\phi\cos\phi + \frac{a_{23}}{\mu}\cos\phi - \frac{a_{13}}{\mu}\sin\phi \tag{4.28}$$

Equations (4.22) and (4.28) form a set of nonlinear differential equations and their analytical solution is not available, and can only be solved numerically. However, qualitative understanding of the equations can be obtained by an analysis of the equations [58]. Equilibrium solutions (a.k.a critical points) give constant solutions of an autonomous system which are

$$\begin{aligned}
\frac{dx_1}{dt} &= f_1\left(x_1, x_2, ..., x_n\right) = 0\\
\frac{dx_2}{dt} &= f_2\left(x_1, x_2, ..., x_n\right) = 0\\
&\vdots\\
&.\\
\frac{dx_n}{dt} &= f_n\left(x_1, x_2, ..., x_n\right) = 0
\end{aligned}$$

After finding constant solution points, nonlinear differential equations can be linearized at those points and the behavior of the equations can be understood by

examining their the geometries. Reducing the system to two differential equations for simplicity and assuming that they have critical points at x^* and y^*, yields

$$\frac{dx}{dt} = f(x^*, y^*) = 0$$
$$\frac{dy}{dt} = g(x^*, y^*) = 0$$

Using tangent plane approximation of $f(x, y)$ at point (x^*, y^*)

$$\frac{dx}{dt} = f(x, y) \approx \underbrace{f(x^*, y^*)}_{0} + \frac{\partial f}{\partial x}(x^*, y^*)\,(x - x^*) + \frac{\partial f}{\partial y}(x^*, y^*)\,(y - y^*)$$

and defining new coordinates u and v

$$u = x - x^* \text{ and } v = y - y^*$$

Since $x^*$and y^* are constants

$$\frac{du}{dt} = \frac{dx}{dt} \text{ and } \frac{dv}{dt} = \frac{dy}{dt}$$

writing linear approximations in terms of u and v gives us:

$$\frac{du}{dt} = \frac{\partial f}{\partial x}|_{x*,y*}\, u + \frac{\partial f}{\partial y}|_{x*,y*}\, v$$

$$\frac{dv}{dt} = \frac{\partial g}{\partial x}|_{x*,y*}\, u + \frac{\partial g}{\partial y}|_{x*,y*}\, v$$

by defining $\mathbf{u} = \begin{bmatrix} u \\ v \end{bmatrix}$, the above equations can be written in matrix form

$$\frac{d\mathbf{u}}{dt} = J\mathbf{u}$$

where J is called Jacobian matrix and it is

$$J = \begin{bmatrix} \frac{\partial f}{\partial x}|_{x*,y*} & \frac{\partial f}{\partial y}|_{x*,y*} \\ \frac{\partial g}{\partial x}|_{x*,y*} & \frac{\partial g}{\partial y}|_{x*,y*} \end{bmatrix}$$

Linearization at the critical points gives qualitatively the same behavior as the nonlinear system if the real parts of the eigenvalues are nonzero. Hence, the

Eigenvalues	Type of critical point
$r_1 > r_2 > 0$	Node
$r_1 < r_2 < 0$	Node
$r_1 < 0 < r_2$	Saddle point

Table 4.1: Stability properties of linear systems

above approach helps explain the "flow" of the impacting bodies. If the imaginary parts of the eigenvalues, r_1 and r_2, are zero, and $r_1 \neq r_2$, the critical point is either a node sink or a saddle point. Node sink is the critical point to which all solutions that start close enough converge as $t \to \infty$ and the saddle point is the critical point where all the solutions depart as $t \to \infty$. Table 4.1 summarizes the stability conditions according to the sign of the eigenvalues, r_1 and r_2. In summary, knowing the Jacobian matrix of the nonlinear set of differential equations at the critical points, provides information on whether the system is stable or not at those points (and additional work gives idea about what happens between these points.)

Focusing back on the flow of the impact, the critical points should be found, which satisfies the following conditions:

$$\frac{ds}{d\tau} = 0 \text{ and } \frac{d\phi}{d\tau} = 0 \tag{4.29}$$

From Equation (4.29) it can be seen that, the critical points, $\bar{s}$ and $\bar{\phi}$ are

$$\bar{s} = 0 \tag{4.30}$$

$$-a_{21}\cos^2\bar{\phi} + a_{12}\sin^2\bar{\phi} + (a_{11} - a_{22})\sin\bar{\phi}\cos\bar{\phi} + \frac{a_{23}}{\mu}\cos\bar{\phi} - \frac{a_{13}}{\mu}\sin\bar{\phi} = 0 \tag{4.31}$$

As mentioned, signs of the eigenvalues of the system's Jacobian matrix at $(\bar{s}, \bar{\phi})$ will tell the behavior of the system, (see Table 4.1).

The flow characteristics have notable points that can provide information about the behavior of the system. One such point is found by setting (Equation 4.28) $d\phi/d\tau = 0$, which gives the invariant directions [58] the conditions where ϕ remains the same (constant) during impact. These lines are called isoclinics and depend on the elements of the mass matrix (i.e. geometry of the impact)

and the friction coefficient. The other is the change in flow directions, which is found from setting $ds/d\tau = 0$ (Equation (4.22)). Using these properties Bhatt and Koechling has tabulated all the posible flow patterns [56–58]

4.1.1.1 Swerve of a 3D Pendulum

Effective matrix for a 3D impact of a pendulum having 2 degrees of freedom was obtained in Equation (4.6) as;

$$B = \begin{bmatrix} a_{11} & a_{12} & a_{13} \\ a_{21} & a_{22} & a_{23} \\ a_{31} & a_{32} & a_{33} \end{bmatrix} = \frac{1}{m} \begin{bmatrix} \cos^2\theta & 0 & \sin\theta\cos\theta \\ 0 & 1 & 0 \\ \sin\theta\cos\theta & 0 & \sin\theta \end{bmatrix} \tag{4.32}$$

writing Equation (4.32) explicitly;

$$M dV_1 = \cos^2\theta dP_1 + \cos\theta\sin\theta dP_3 \tag{4.33}$$

$$M dV_2 = dP_2 \tag{4.34}$$

$$M dV_3 = \sin\theta\cos\theta dP_1 + \sin^2\theta dP_3 \tag{4.35}$$

From Equations (4.22) and (4.28) radial and angular components of the tangential velocity for the pendulum can be obtained as:

$$\frac{ds}{d\tau} = s\left(\frac{\sin\theta\cos\theta}{\mu}\cos\phi - \cos^2\phi - \cos^2\theta\cos^2\phi - \sin^2\phi\right) \equiv f \tag{4.36}$$

$$\frac{d\phi}{d\tau} = \left(\cos^2\theta - 1\right)\sin\phi\cos\phi - \frac{1}{\mu}\sin\theta\cos\theta\sin\phi \equiv g \tag{4.37}$$

critical points, $\bar{s}, \bar{\phi}$, are found using Equations (4.36) and (4.37)

$$\bar{s} = 0$$

$$\bar{\phi} = \left(\cos^2\theta - 1\right)\sin\phi\cos\phi - \frac{1}{\mu}\sin\theta\cos\theta\sin\phi = 0$$

linearizing Equations (4.36) and (4.37) at critical points

$$\frac{ds}{d\tau} = f(s,\phi) \text{ and } \frac{d\phi}{d\tau} = g(s,\phi)$$

and using tangent plane approximation yields

$$\frac{ds}{d\tau} = f(s,\phi) \approx f(\bar{s},\bar{\phi}) + \frac{\partial f}{\partial s}|_{\bar{s},\bar{\phi}}\,(s-\bar{s}) + \frac{\partial f}{\partial \phi}|_{\bar{s},\bar{\phi}}\,(\phi-\bar{\phi})$$

$$\frac{d\phi}{d\tau} = g(s,\phi) \approx g(\bar{s},\bar{\phi}) + \frac{\partial g}{\partial s}|_{\bar{s},\bar{\phi}}\,(s-\bar{s}) + \frac{\partial g}{\partial \phi}|_{\bar{s},\bar{\phi}}\,(\phi-\bar{\phi})$$

Defining $u = s - \bar{s}$ and $v = \phi - \bar{\phi}$ and noting that $\bar{s}$ and $\bar{\phi}$ are constants leads to

$$\frac{du}{d\tau} = \frac{ds}{d\tau}\ ,\ \frac{dv}{d\tau} = \frac{d\phi}{d\tau}$$

$$\frac{du}{d\tau} = \frac{\partial f}{\partial s}|_{\bar{s},\bar{\phi}}\,u + \frac{\partial f}{\partial \phi}|_{\bar{s},\bar{\phi}}\,v$$

$$\frac{dv}{d\tau} = \frac{\partial g}{\partial s}|_{\bar{s},\bar{\phi}}\,u + \frac{\partial g}{\partial \phi}|_{\bar{s},\bar{\phi}}\,v$$

and in matrix form

$$\begin{bmatrix} du/d\tau \\ dv/d\tau \end{bmatrix} = J \begin{bmatrix} u \\ v \end{bmatrix} \tag{4.38}$$

$$J = \begin{bmatrix} \frac{\partial f}{\partial s}|_{\bar{s},\bar{\phi}} & \frac{\partial f}{\partial \phi,}|_{\bar{s},\bar{\phi}} \\ \frac{\partial g}{\partial s}|_{\bar{s},\bar{\phi}} & \frac{\partial g}{\partial \phi}|_{\bar{s},\bar{\phi}} \end{bmatrix} \tag{4.39}$$

where the elements of Equation (4.39) can be written as

$$\frac{\partial f}{\partial s}|_{\bar{s},\bar{\phi}} = \frac{1}{\mu}\sin\theta\cos\theta\cos\bar{\phi} - \cos^2\theta\cos^2\bar{\phi} - \sin^2\bar{\phi} \tag{4.40}$$

$$\frac{\partial f}{\partial \phi}|_{\bar{s},\bar{\phi}} = 0 \tag{4.41}$$

$$\frac{\partial g}{\partial s}|_{\bar{s},\bar{\phi}} = 0 \tag{4.42}$$

$$\frac{\partial g}{\partial \phi}|_{\bar{s},\bar{\phi}} = \left(\cos^2\theta - 1\right)\left(\cos^2\bar{\phi} - \sin^2\bar{\phi}\right) - \frac{1}{\mu}\sin\theta\cos\theta\,\cos\bar{\phi} \tag{4.43}$$

If the eigenvalues of the given Jacobian are known, stability condition of the critical point can be estimated from Table 4.1 from the signs of eigenvalues.

Consider an impact of a pendulum that makes $\theta = 60^o$ angle with vertical, with a unit mass is unity and a friction coefficient, $\mu = 1$.

Starting with finding the critical points with $g = 0$ and $f = 0$. Since for $\bar{s} = 0$ for each critical point these also represents invariant directions from $g = 0$. The roots are as follows:

$\bar{s}, \bar{\phi}$	r_1	r_2	Stability condition
0,0	-1.18	0.18	Saddle
0,2.18	-1	0.5	Saddle
0,π	-0.68	-0.32	Node
0,4.09	-1	0.5	Saddle

Table 4.2: Eigenvalues for $\theta = 60^o$ and $\mu = 1$

$\bar{\phi}_1 = 0,\ \bar{\phi}_2 = 2.1862,\ \bar{\phi}_3 = \pi,\ \bar{\phi}_4 = 4.0967$

Then from Equation (4.36), with $f = 0$, find flow change of flow directions are found as:

$\hat{\phi}_1 = 0.4474,\ \hat{\phi}_2 = 5.8357$

For each critical point, corresponding eigenvalues are tabulated in Table 4.2

In [57] the flow behavior is classified based on the numbers of invariant directions, flow change directions, saddle points and node sinks. The flow field for the examples of the pendulum is obtained with MATLAB and the result is presented in Figure 4.2. In Figure 4.2 solid lines show the invariant directions and dashed lines show the flow change directions. Seperatrix and isoclinic lines where the flow is diverged and converged, respectively can be observed and this information can be used to estimate the motion of the 3D pendulum.

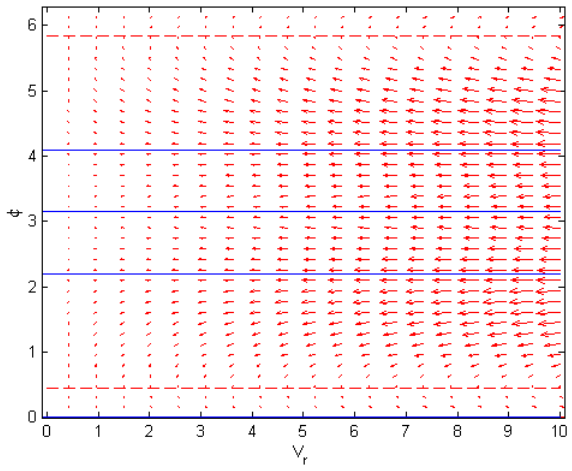

Figure 4.2: Flow field of a 3D pendulum with $\mu = 1$ and $\theta = 60^o$

4.2 Impact of a 2D Pendulum

If rotations of the pendulum about $\mathbf{n}_3$ and $\mathbf{n}_1$ are constrained, the motion becomes planar and has a two-dimensional motion. Planar impact of a pendulum is analysed by many authors because of its simplicity to explain complex phenomena related to constrained impacts. For instance, Lubarda [36] uses a rigid planar pendulum to show the bounds of different definitions of coefficient of restitution, Glocker and Pfeiffer [15] explain frictional impact and introduces the subject with a rigid pendulum. Ivanov [7] solves an example using a pendulum, which has deformable elements both at the contact point and at the hinge. Since in this thesis equations related to dynamics of a physical pendulum will be used, related equations will be derived in detail below using the basic dynamical relations. In the following derivations, a physical pendulum described by a solid sphere connected to point O with massless connection, will be used.

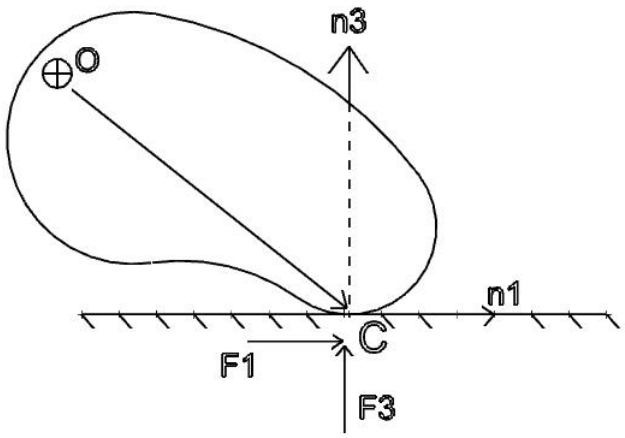

Figure 4.3: Schematic representation of a planar pendulum

As presented in Figure 4.3, $\mathbf{n_1}$ represents the tangential direction and $\mathbf{n_3}$ shows the normal direction. The pendulum pivots about $\mathbf{n_2}$ and the contact is assumed to occur at point C.

From Figure 4.3, moments about point O is:

$$J_{22}\ddot{\theta} = F_3 L \sin\theta + F_1 L \cos\theta \tag{4.44}$$

where J_{22} is the moment of inertia about point O. For the physical pendulum used as the impacting body,

$$J_{22} = \frac{2}{5}mR^2 + mL^2 \tag{4.45}$$

Substituting J_{22} in Equation (4.44) becomes

$$\left(\frac{2}{5}mR^2 + mL^2\right)\ddot{\theta} = F_3 L\sin\theta + F_1 L\cos\theta \tag{4.46}$$

The angular velocity of the pendulum, $\dot{\theta}$, can be calculated using this components of linear velocity, V:

$$V = \sqrt{\dot{x}^2 + \dot{z}^2} = \dot{\theta}L \tag{4.47}$$

where

$$\dot{x} = L\cos\theta\,\dot{\theta} \tag{4.48}$$

$$\dot{z} = L\sin\theta\,\dot{\theta} \tag{4.49}$$

with the corresponding accelerations:

$$\ddot{x} = -L\sin\theta\,\dot{\theta}^2 + L\cos\theta\,\ddot{\theta} \tag{4.50}$$

$$\ddot{z} = L\cos\theta\,\dot{\theta}^2 + L\sin\theta\,\ddot{\theta} \tag{4.51}$$

The equation of motion in tangential direction, $\mathbf{n_1}$, becomes:

$$\ddot{\theta} = \frac{\dot{x} + L\sin\theta\,\dot{\theta}^2}{L\cos\theta} \tag{4.52}$$

Using Equation (4.52) in Equation (4.46)

$$\left(\frac{2}{5}mR^2 + mL^2\right)\left\{\frac{\ddot{x} + L\sin\theta\,\dot{\theta}^2}{L\cos\theta}\right\} = F_3 L\sin\theta + F_1 L\cos\theta \tag{4.53}$$

$$\ddot{x} + L\sin\theta\,\dot{\theta}^2 = \frac{5}{m\left(2R^2 + 5L^2\right)}L^2\cos^2\theta\,F_1 + \frac{5}{m\left(2R^2 + 5L^2\right)}L^2\sin\theta\,\cos\theta\,F_3 \tag{4.54}$$

For the equation of motion in normal direction, from Equaiton (4.51)

$$\ddot{\theta} = \frac{\ddot{z} - L\cos\theta\,\dot{\theta}^2}{L\sin\theta} \tag{4.55}$$

using this in Equation (4.46)

$$\left(\frac{2}{5}mR^2 + mL^2\right)\left\{\frac{\ddot{z} - L\cos\theta\,\dot{\theta}^2}{L\sin\theta}\right\} = F_3 L\sin\theta + F_1 L\cos\theta \tag{4.56}$$

$$\ddot{z} - L\cos\theta\,\dot{\theta}^2 = \frac{5}{m\left(2R^2+5L^2\right)}L^2\sin\theta\,\cos\theta F_1 + \frac{5}{m\left(2R^2+5L^2\right)}L^2\sin^2\theta F_3 \tag{4.57}$$

and in matrix form the equation that define motion of the pendulum become

$$\left\{\begin{array}{c} d^2x/dt^2 \\ d^2z/dt^2 \end{array}\right\} = \left[\begin{array}{cc} \frac{5}{m(2R^2+5L^2)}L^2\cos^2\theta & \frac{5}{m(2R^2+5L^2)}L^2\sin\theta\,\cos\theta \\ \frac{5}{m(2R^2+5L^2)}L^2\sin\theta\,\cos\theta & \frac{5}{m(2R^2+5L^2)}L^2\sin^2\theta \end{array}\right]\left\{\begin{array}{c} F_1 \\ F_3 \end{array}\right\} \tag{4.58}$$

4.2.1 2D Pendulum with Compliant Elements at the Contact

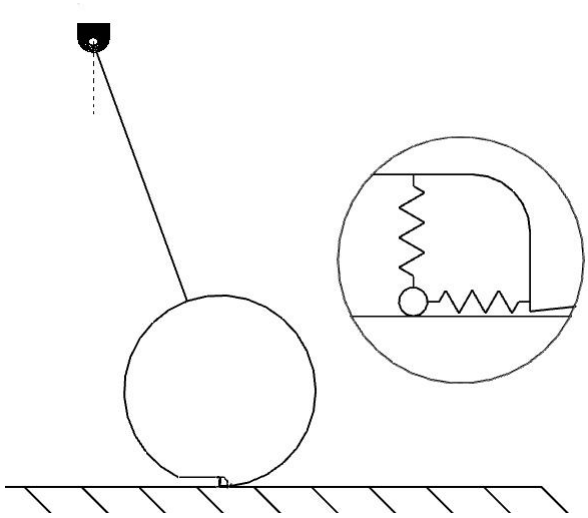

Figure 4.4: Schematic representation of the physical pendulum and compliant elements

Behavior of a pendulum colliding with a massive plate is similar to a free oblique impact of a sphere, except that the pendulum is constrained at a hinge. Constrained motion of the pendulum complicates the problem, since after the impact, has a constrained direction. Furthermore, its restitution phase is influenced by friction during contact.

On developing and using the equations of motion for the pendulum, the assumptions related to the system and collision are as follows:

• A physical pendulum defined as a solid sphere connected to a pivot point O, with a massless link, collides on a massive surface for the following analysis.

• Two compliant elements in normal and tangential directions are used between the contact point and the body.

• The stiffness of the joint at the pivot O is infinite and any energy dissipation at this connection is neglected. Also, the impact is assumed to be perfecty elastic. Hence, the only dissipation mechanism is friction at the impact region. Other means of dissipation, such as wave propagation and structural damping are neglected.

• Coefficient of friction is constant and independent of transitions between sticking and sliding phases.

• Effect of change in the impact angle during collision is so small that effective mass matrix, $\boldsymbol{B}$ is assumed to remain constant throughout impact.

• Effect of the weight of the pendulum on the dynamics of the system is neglected, since the gravitational forces are small compared to impact forces.

4.2.1.1 Dynamics of the System

4.2.1.1.1 Derivation of Inertia Matrix Inertia matrix, $\mathbf{B}$, in the impulse-momentum relation, $\mathbf{\Delta V_R} = \mathbf{BP}$, for planar configuration is presented in Section 4.2 for a physical pendulum of length L with a solid sphere of radius, R, at its. The equations of motion, expressed in tangential and normal directions are given in Equation (4.58) such that

$$\left\{ \begin{array}{c} d^2x/dt^2 \\ d^2z/dt^2 \end{array} \right\} = \boldsymbol{B} \left\{ \begin{array}{c} F_1 \\ F_3 \end{array} \right\}$$

where

$$\boldsymbol{B} = \begin{bmatrix} a_{11} & a_{13} \\ a_{31} & a_{33} \end{bmatrix} = \begin{bmatrix} \frac{5}{m(2R^2+5L^2)} L^2 \cos^2\theta & \frac{5}{m(2R^2+5L^2)} L^2 \sin\theta\, \cos\theta \\ \frac{5}{m(2R^2+5L^2)} L^2 \sin\theta\, \cos\theta & \frac{5}{m(2R^2+5L^2)} L^2 \sin^2\theta \end{bmatrix} \tag{4.59}$$

4.2.1.1.2 Force-Displacement Relations As discussed in Section 3.3.1.1.2, linear springs are used to represent the compliance of the body. Behavior of the system is affected by the ratios of the stiffnesses, $\eta = k_3/k_1$ of the elements and this ratio varies between 1.17 to 1.5 as the Poisson's ratio varies from 0.25 to 0.5 [16]. Throughout the thesis generally $\eta = 1.21$ will be employed, however, other values for this ratio will also be used in the following sections to investigate when the tangential compliance is negligible (rigid-body assumption). Relations given in Equations (3.44, 3.45) will be used for force-displacement relations.

$$F_1 = -k_1 u_1 \tag{3.44}$$

$$F_3 = -k_3 u_3 \tag{3.45}$$

As defined previously, during impact two types of contact develop: sticking and sliding. Different equations describe the pendulum motion for the two cases as shown below.

4.2.1.1.3 Equations for Stick Since the contact point is attached to the surface during stick, tangential velocity of the body becomes equal to the rate of change of the of the tangential spring's length, i.e. $dx/dt = du_1/dt$. As a result, Equations (3.44) and (3.45) are used in Equation (3.41).

$$\begin{Bmatrix} d^2x/dt^2 \\ d^2z/dt^2 \end{Bmatrix} = \begin{Bmatrix} d^2u_1/dt^2 \\ d^2u_3/dt^2 \end{Bmatrix} = \begin{bmatrix} -a_{11}k_1 & -a_{13}k_3 \\ -a_{31}k_1 & -a_{33}k_3 \end{bmatrix} \begin{Bmatrix} u_1 \\ u_3 \end{Bmatrix} \tag{3.47}$$

Equation (3.47) with related initial conditions of u_1, u_3, $\dot{u}_1$ and $\dot{u}_3$, describes the motion of the pendulum during sticking.

4.2.1.1.4 Equations for Sliding During sliding, displacements u_1 and u_3 are related to each other through Amontons-Coulomb law $F_1 = -\mu\hat{s}F_3$. Hence, the differential equation (3.43), which is a function of u_3 can be solved making use of the linear relations of displacement and force in Equation (3.45) . Note that the normal velocity of the body is the same as the rate of displacement of the normal spring during the impact period, leading to:

$$\frac{d^2u_3}{dt^2} = m^{-1}\left(a_{31}\mu\hat{s} - a_{33}\right)k_3u_3 \tag{3.49}$$

Solving Equation (3.49) with initial conditions for u_3 and $\dot{u}_3$, gives the normal motion of the body. With u_3, $\dot{u}_3$ and Equation (3.48), tangential components can be found and are given in Equations (3.50) and (3.51) as

$$u_1 = -\frac{k_3}{k_1}\mu\hat{s}u_3 \tag{3.50}$$

$$\dot{u}_1 = -\frac{k_3}{k_1}\mu\hat{s}\dot{u}_3 \tag{3.51}$$

Whether the impact is initially sticking or sliding is determined from a combination of the ratio of the initial normal and tangential velocities, friction coefficient and stiffness ratio. The limiting condition for initially sliding or sticking behavior is given in Section 3.3.1.1.6 by Equation (3.53) as

$$\left|\frac{\dot{x}(0)}{\dot{z}(0)}\right| < \mu\frac{k_3}{k_1} \tag{3.53}$$

For the pendulum problem, the inequality in Equation (3.53)corresponds to

$$\cot\theta < \mu\frac{k_3}{k_1} \tag{4.60}$$

where θ is the angle between the pendulum and normal.

4.2.1.1.5 Initially Sticking Case In the pendulum impact problem it is important to delineate the terms "stick" and "wedge", which describe different conditions. Stick refers to the condition of the contact point where the contact point is attached to the surface even when the body continues its motion. Wedging refers to the condition when the colliding body can not rebound at the

end of the collision and system is locked. Wedging for rigid body assumption was discussed in detail in the previous chapter and will be discussed below when compliance is considered in the model.

If the inequality in Equation (4.60) is satisfied, contact point initially sticks and the differential equations (3.47) for sticking are solved with $u_1(0) = 0$, $u_3(0) = 0$, $\dot{u}_1(0)$ and $\dot{u}_3(0)$. In this case, $\dot{u}_1(0)$ and $\dot{u}_3(0)$ are equal to the components of the initial velocity of the body, respectively. If the pendulum is stuck, it means that tangential force created by the impact can not overcome friction and the tangential compliance in the material allows the body to continue moving, unlike with the rigid body assumption. When using rigid-body assumption, if the external forces on the body are less than the friction force, the body can not move. However if compliance is considered, the body acts as if it is colliding with springs in both normal and tangential directions. Unlike the free impact of a solid sphere or oblique impact of a rod, sticking does not follow sliding. Hence, impact of a simple pendulum does not include reversal of the tangential force (if initial stick occurs). Sticking during the impact is not encountered in free collisions and will be named "gross stick" in this thesis.

Results from an example of such an impact are presented in Figure 4.5. On left-hand side of the Figure 4.5, dashed lines describe the normalized normal force envelope, solid line the normalized tangential force, and the thin line shows the tangential velocity, $\dot{x}$, respectively. On right-hand side, normalized normal velocity of the body, $\dot{u}_3/\dot{z}(0) = \dot{z}/\dot{z}(0)$, normalized velocity of the tangential element, $\dot{u}_1/\dot{z}(0)$, normalized sliding velocity, $s/\dot{z}(0) = (\dot{x} - \dot{u}_1)/\dot{z}(0)$, and normalized velocity of the body, $\dot{x}/\dot{x}(0)$ are shown.

As seen from the figure, normal and tangential forces act on the body with the same frequency making the sliding transition and reversal impossible. Since during sticking, friction force does not do any work there is no energy dissipation. The fact that the system does not lose any energy can also be seen from the normalized velocity plots of Figure 4.5. From $\dot{z}/\dot{z}(0)$ and $\dot{u}_3/\dot{x}(0)$ plots, it can be seen that final and initial velocities are equal. In addition, when there is no sliding, friction force does not do any work since displacement in tangential direction is

zero. Sliding velocity plot of Figure 4.5 indicates that during sticking $s = 0$, meaning sliding does not occurs during impact. Also, since point c is attached to the surface, tangential displacements of the body, x and the displacement of the compliant element, u_1 are equal.

In the the left-hand side plot of Figure 4.5, tangential force is normalized by dividing it with μ, such that if $F_1 = \mu F_3$ values coincide. However, during sticking portion of impact, this equality is not satisfied. Tangential force is always less than the limiting friction force, μF_3 to slide. This behavior is classified as "gross stick" in Figure 3.2. Displacements of spring elements, u_1 and u_3 are also presented in Figure 4.5 to illustrate their variation with velocity. It can be seen that at the beginning of impact, spring elements start to compress. Pendulum moves inward, θ decreaes, as the velocity of the pendulum is decreases. When all the initial energy of the pendulum is transferred to the compliant elements, u_1 and u_3 reach their maximum values and $\dot{x}$ and $\dot{z}$ vanish. After this point, restitution starts and the energy stored in the springs are transferred back to the body, and the velocity of the pendulum increases until the conclusion of the impact.

4.2.1.1.6 Initially Sliding Case If the tangential force overcomes friction force, sliding is initiated and the inequality in (3.53) can be related to geometry via $\cot\theta > \mu k_3/k_1$. Geometrically this corresponds to smaller pendulum angles. The behavior of the pendulum can be better understood by examining the forces and the velocities and are presented in Figure 4.6. Solution of Equation (3.49) with $u_3(0) = 0$ and $\dot{u}_3(0) = \dot{z}(0)$ gives time-dependent values of normal components of displacement and velocity, from which the tangential components and forces can be calculated as explained previously. For the time, t_{lt}, of transition from sliding to sticking, the time when the sliding speed, s, vanishes is found, i.e. $s = 0$ corresponds to initiation of sticking. Then, the sticking equations given in Equation (3.47) are solved numerically using $u_1(t_{lt})$, $u_3(t_{lt})$, $\dot{u}_1(t_{lt})$ and $\dot{u}_3(t_{lt})$ as initial conditions. Solution of the differential equation (3.47) gives time-dependent normal and tangential components of velocity and displacements. Sticking continues until $t = t_{tl}$ where tangential force overcomes friction force,

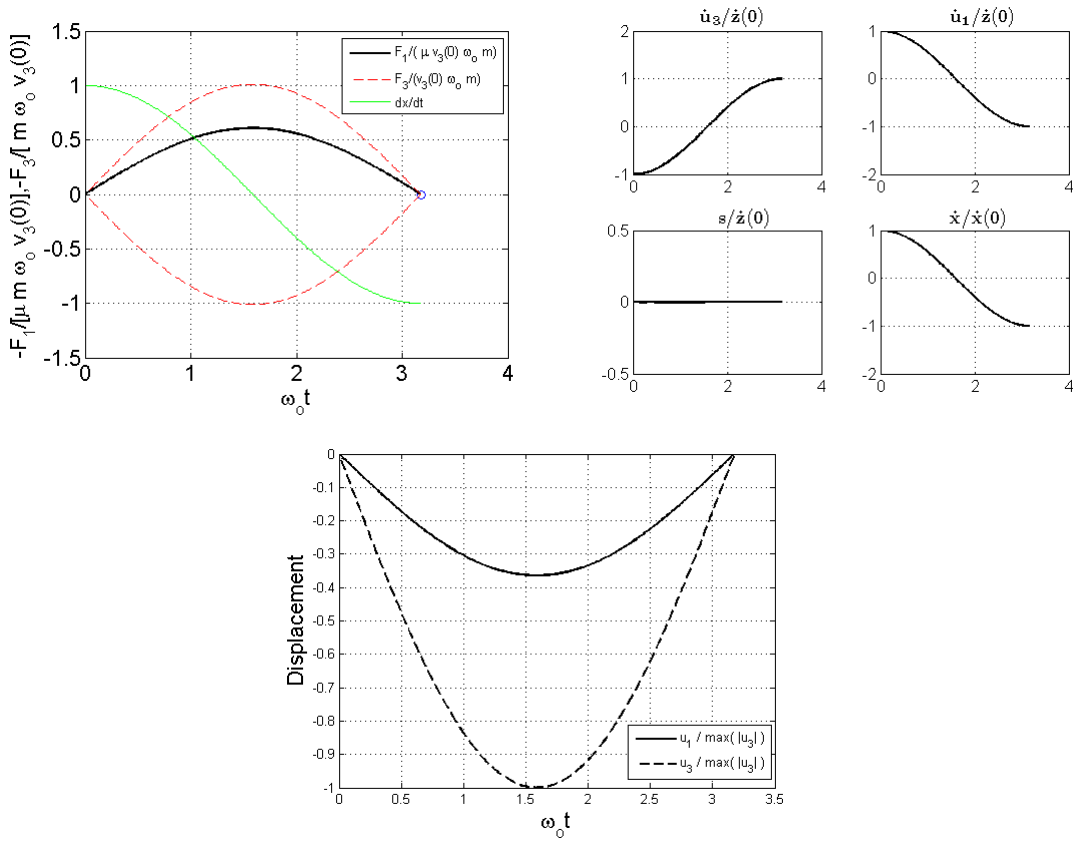

Figure 4.5: Initial sticking of a pendulum with $\mu = 0.5$, $\theta = 70^o$, $V_1(0)/V_3(0) = 2.75$, and $k_3/k_1 = 1.21$,$R = 5 \times 10^{-3}\, m$,$L = 0.1\, m$

μF_3, and sliding initiates at $t = t_{tl}$. During sliding, again, solution of Equation (3.49) with $u_3(t_{tl})$ and $\dot{u}_3(t_{tl})$, displacements and velocities are calculated.

In Figure 4.6, left-hand side plot shows the normalized tangential and normal forces. Normalized spring displacements, u_1 and u_3, are also presented in Figure 4.6. The results show as before, at the beginning of the impact the compliant elements start to compress and the velocity of the body decreases. Similar to the gross stick case, pendulum stops when displacements of the spring elements reach their maximum values. Until the end of the compression of the compliant elements, pendulum continues to move inward, with θ decreasing. When the pendulum stops, stick starts and pendulum starts to reverse its direction, which is indicated in Figure 4.6 with the change of sign of the velocity. Just after the velocity reversal, point C becomes attached to the surface and the body releases the compressed tangential spring element. In other words, compressed spring starts to push the pendulum after sticking starts. In this phase, velocity of the pendulum increases. After some time, length of spring element returns to its initial length ($u_1 = 0$ where the tangential displacement reaches zero) and the pendulum starts to elongate the spring while point C is still attached to the surface. At $t = t_{tl}$, the spring is stretched enough to overcome the friction force and sliding starts again. During sliding, friction force performs work against the motion of the pendulum causing energy loss. The energy loss can be observed in velocity plots, noting that $\dot{u}_3(t_f)/\dot{z}(0)$ and $\dot{x}(t_f)/\dot{x}(0)$ are less than their initial values. In the $\dot{u}_1/\dot{z}(0)$ plot of Figure 4.6, the jump in the velocity at the transition from sticking to sliding can also be seen. Also, zero sliding velocity during sticking and motion direction of the pendulum can be seen in the $s/\dot{z}(0)$ plot.

4.2.1.2 Effects of Change of Variables

After discussing the general trends in impact of a pendulum with compliant elements model, the effects of variables of the system are discussed. Figure 4.7 shows normalized forces and tangential velocities for different μ while other parameters are held constant. Normalized normal and tangential force plots on the left-hand side of Figure 4.7 show that as friction coefficient decreases duration of impact

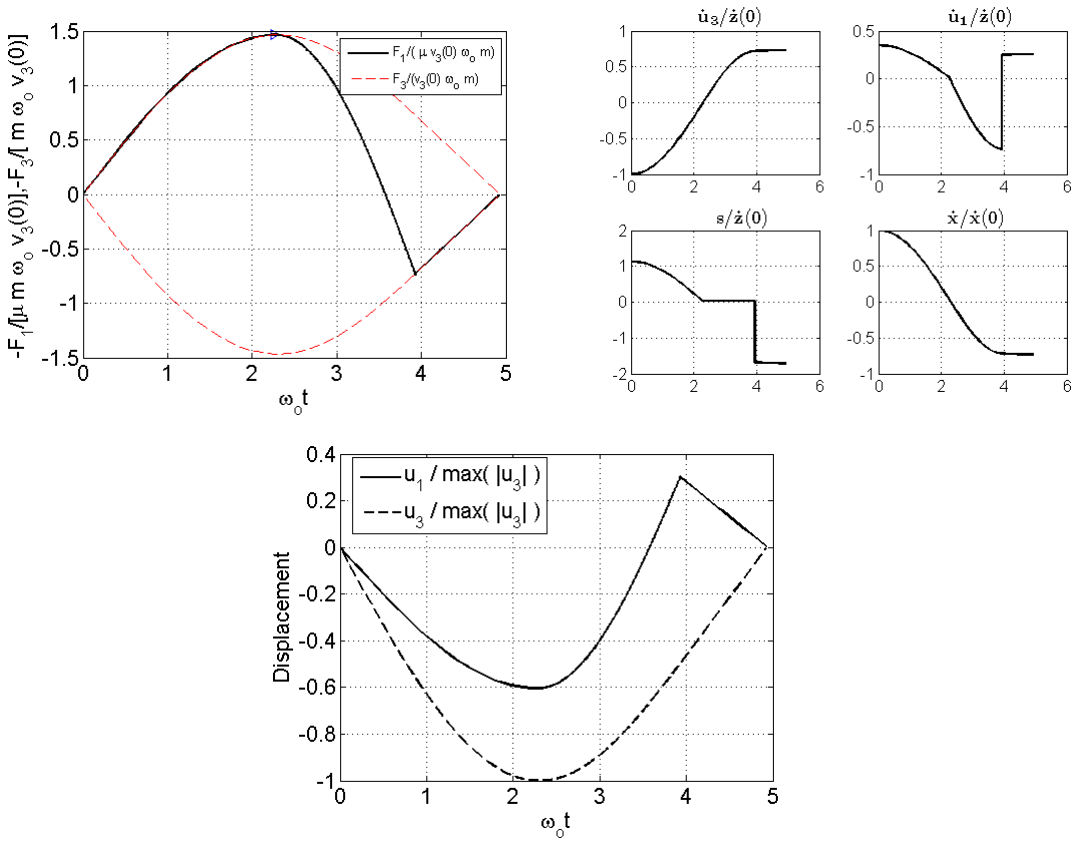

Figure 4.6: Initial sliding of a physical pendulum with $\mu = 0.5$, $\theta = 30^o$, $V_1(0)/V_3(0) = 1.73$, $k_3/k_1 = 1.21$, and $R = 5 \times 10^{-3}\, m$, $L = 0.1\, m$

increases. The final tangential velocities at the left-hand side plot of Figure 4.7, show that friction coefficient and final velocity are not linearly related for the same impact angle, θ, and same impact velocity, . From the first impression, it can be said that, losses are directly related to coefficient of friction, hence increase in μ should increase the losses. However, losses during an elastic impact are not only related to friction force but also related to amount of displacement and this will be discussed in the following section in detail.

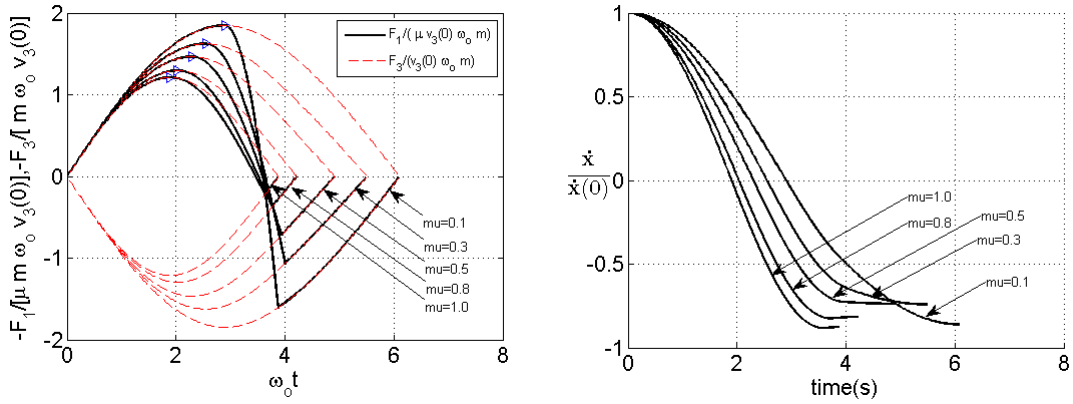

Figure 4.7: Effect of change of μ with $\mu = 0.1, 0.3\,0.5, 0.8$ and 1.0, $\theta = 30^o$, $V_1(0)/V_3(0) = 1.73$, $k_3/k_1 = 1.21$, $R = 5 \times 10^{-3}\,m$, and $L = 0.1\,m$

Another important variable of the system is the angle, θ, that the pendulum makes with the normal. Effects of angle of impact on the system will be shown while other parameters held constant in Figure 4.8. On the left-hand side, normalized forces are shown and it can be seen that, as θ is increased, initially sticking impact is initiated instead of initially sliding impact. Considering the geometry of the pendulum, for smaller impact angles, friction coefficient necessary for wedging is also smaller because of the increasing dissipation in the system. Increasing dissipation with decreasing θ can be seen from tangential velocity plot presented on the right hand side. In addition, duration of the impact is higher with smaller collision angles, later it will be shown that when θ is less than a critical value, the duration of the impact goes to infinity implying that the contact is permanent, which was defined as wedging in the previous sections.

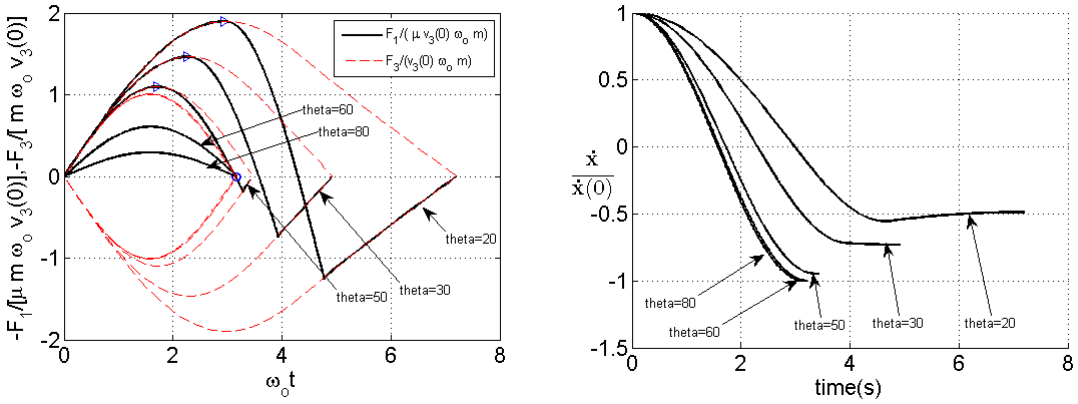

Figure 4.8: Effect of change of θ with $\theta = 20$, 30, 50, 60 and 80^o $\mu = 0.5$, and $k_3/k_1 = 1.21$

4.2.1.3 Dissipation of Energy

The collision of the pendulum is assumed to be perfectly elastic, i.e. the system does not lose any energy because of yielding, damping etc. On the other hand, friction force produces dissipation and this forms the only energy dissipation mechanism in the system.

To distinguish between the work of the *tangential force* and the *friction force* consider, sticking phase of the pendulum during which, displacement of the contact point is zero, hence friction force does not perform work. On the other hand, the pendulum continues to move, but because of the perfect elasticity in the system, all the initial energy is recovered at the end of the impact. Figure 4.9 displays work by tangential component of the work, denoted by subscript '1', and normal component of the work, denoted by subscript '3'. Partial work done during compression and restitution phases can be calculated from the area under F_iV_i curves such that:

$$W_{ic} = \int_0^{t_c} F_i V_i dt \qquad i = 1, 3 \tag{4.61}$$

$$W_{ir} = \int_{t_c}^{t_f} F_i V_i dt \qquad i = 1, 3 \tag{4.62}$$

where t_c denotes the time at the end of the compression phase. In Figure 4.9

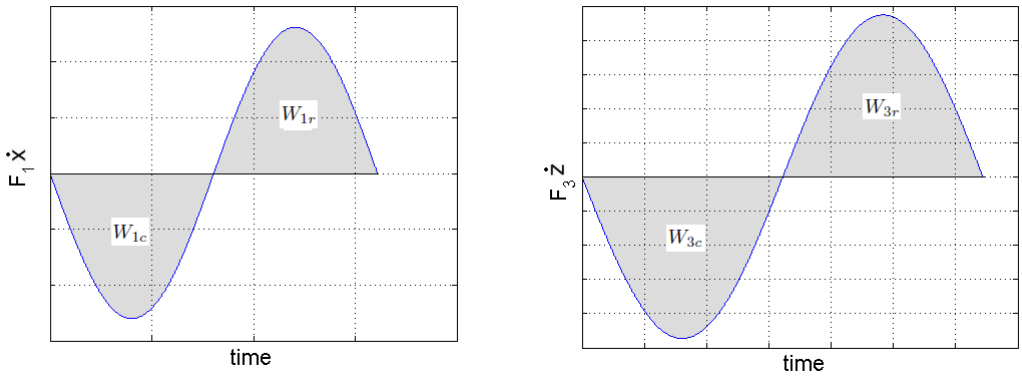

Figure 4.9: Work done during initially sticking case of the pendulum

negative work represents that during compression, and during restitution the same energy is gained with positive work, i.e. $W_{1c} + W_{1r} = 0$ and $W_{3c} + W_{3r} = 0$. Velocity plots presented in Figure 4.5, where initial and final normal and tangential velocities are equal, are consistent with this result.

Initial sliding condition is somewhat different than sticking, since friction does negative work that is not recovered. Until the initiation of sticking, $t = t_{lt}$, both friction and tangential forces do negative work. During sticking, $t_{lt} < t < t_{tl}$, friction does not do any work, since $s = 0$, but tangential force does positive work recovering some of the energy transferred to the compliant elements. At the time where $u_1 = 0$, tangential force starts negative work again since tangential compliant element is elongating and absorbing energy. At $t = t_{tl}$, friction force starts negative work while work of tangential force is still negative. In Figure 4.10 tangential and normal work done during collsion are presented. Again, work done by the normal force during compression is equal to that by the normal force during restitution because of the perfectly elastic assumption. A comparison of elactic and dissipated energies are presented in Figure 4.10, calculated as:

$$W_{11} = \int_0^{t_{lt}} F_1 \dot{x} dt \tag{4.63}$$

$$W_{13} = \int_{t_{lt}}^{t_{tl}} F_1 \dot{x} dt \tag{4.64}$$

$$W_{12} = \int_{t_{tl}}^{t_f} F_1 \dot{x} dt \tag{4.65}$$

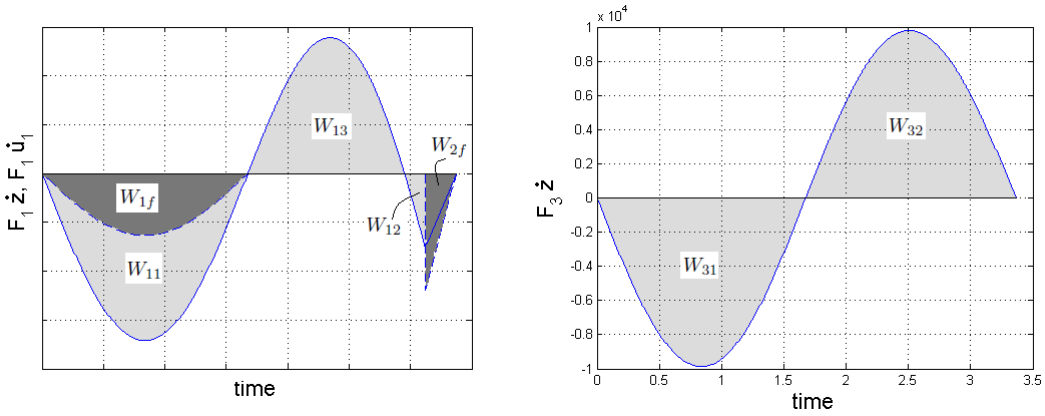

Figure 4.10: Work done during initially sliding case of the pendulum

$$W_{1f} = \int_0^{t_{lt}} F_1 s dt \tag{4.66}$$

$$W_{2f} = \int_{t_{tl}}^{t_f} F_1 s dt \tag{4.67}$$

To sum up, in the initially sliding case of impact of a pendulum, friction force always does negative work dissipating energy whereas tangential force does both positive (if velocity of the body and the tangential force acting in the same direction) and negative work. The total dissipated energy can be calculated as:

$$T_o - T_f = \frac{1}{2}mV(0)^2 - \frac{1}{2}mV(t_f)^2 = W_{1f} + W_{2f} = W_{11} + W_{13} + W_{12} \tag{4.68}$$

where T_o and T_f represents the initial and final kinetic energy of the pendulum respectively and $V(t)$ denotes the resultant velocity, i.e. $V(t) = \sqrt{\dot{x}(t)^2 + \dot{z}(t)^2}$.

Another issue mentioned during discussion on the effect of μ was the fact that a decrease in final velocity is not linearly related to an increase in friction coefficient at a specific impact angle, θ. This can be explained from the friction force and sliding velocity relationship. Because of the nonlinear dynamics of the problem, maximum dissipation occurs somewhere between maximum and minimum friction coefficients when the stiffness ratios, k_3/k_1 have values close to physically realistic values. Figure 4.11 displays change of normalized dissipation and final velocity as a function of μ for as stiffness ratio of $k_3/k_1 = 1.21$. As expected, minimum final velocity is seen at the friction coefficient value where maximum energy dissipation

due to friction is observed. Figure 4.12 shows normalized energy dissipation and final velocity changes with μ for lower k_3/k_1. However, for this case trend is nearly linear; dissipation increases and final velocities decrease with increasing friction coefficient. The differences observed for low and high stiffness ratios also appear in the development of wedging and this will be discussed in the following section.

4.2.1.4 Comparison of Compliant Elements Model with Classical Impact Theory

Knowing the initial velocity of the colliding pendulum, its final velocity can be calculated with the classical impact theory via energetic coefficient of restitution with the following equation

$$\dot{\theta}(t_f) = -e_* \, \dot{\theta}(0) \, \frac{x^2 - \mu x z}{x^2 + \mu x z} \tag{4.69}$$

where e_* is energetic coefficient of restitution (COR), which is the "ratio of square root of internal energy of deformation released at contact point during restitution to the corresponding energy gained during compression" [1], and will be taken as 1 without any irreversible deformation assumption. "Rigid body assumption" refers to negligible compliance, hence there is no stick phase during impact and contact point slides throughout the collision and reversal of the direction occurs just after the angular velocity vanishes. The comparison for different values of k_3/k_1 and θ with changing μ is presented in Figure 4.13 using resultant linear velocities, $V = \sqrt{\dot{x}^2 + \dot{z}^2}$ or $V = \dot{\theta} L$ for both methods. From Figure 4.13 it can be seen that, final velocities calculated with COR is always less than the results obtained with compliant elements method. For very low stiffness ratios the results for final velocity converge to values above the rigid-body case, but apporach it near wedging conditions at lower angles of incidence see $\theta = 10^o$ case in Figure 4.13. However, the difference decreases close to the critical coefficient of friction which is the limiting value for wedging at a specified angle, θ.

Tangential compliance in the system raises the possibility of sticking during impact. As mentioned previously, according to compliant elements model,

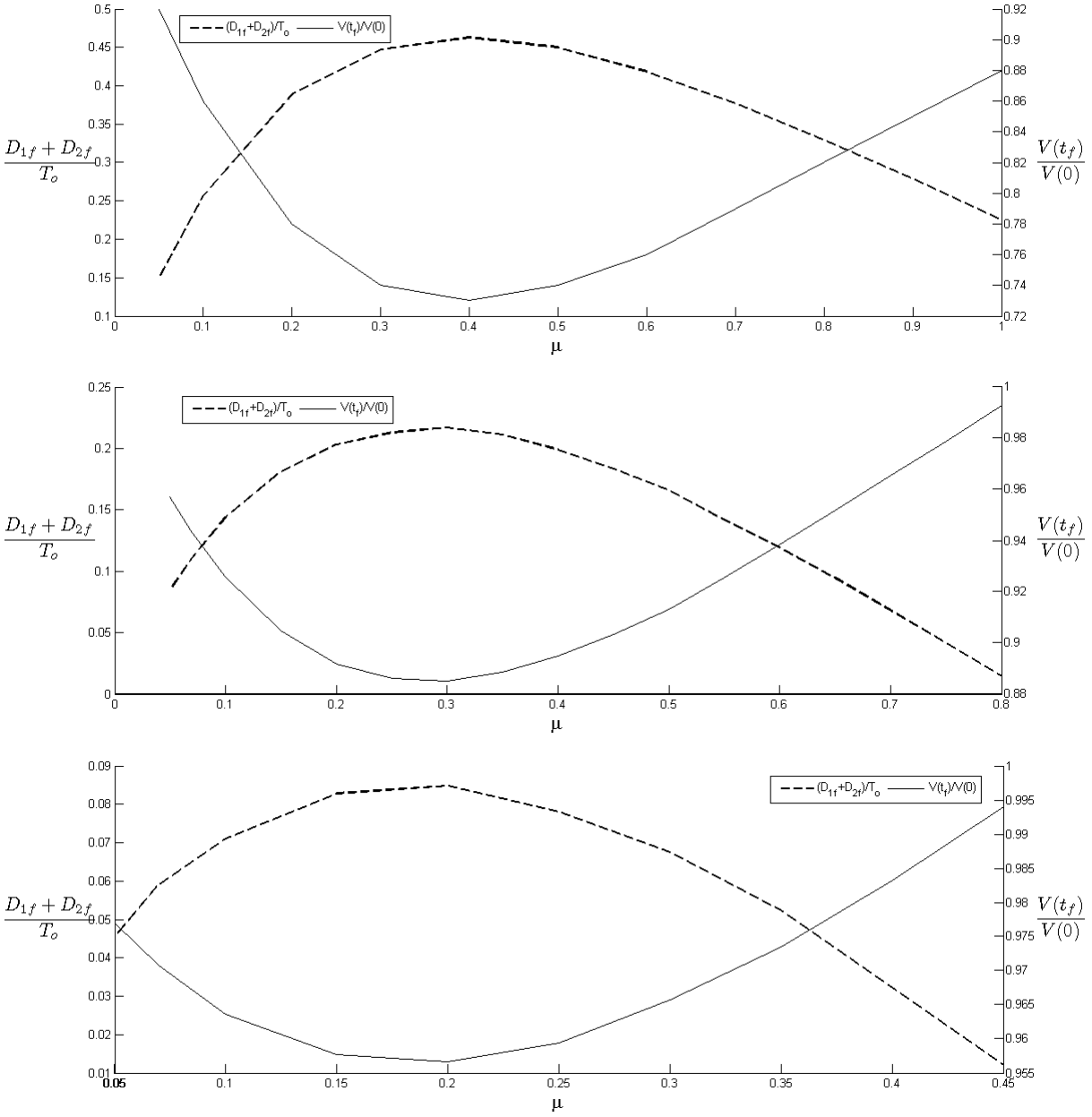

Figure 4.11: Frictional dissipation and final velocities during initially sliding impact of pendulum for different angles of impact, $\theta = 30,\ 45,\ 60^o$ top to bottom for $k_3/k_1 = 1.21$

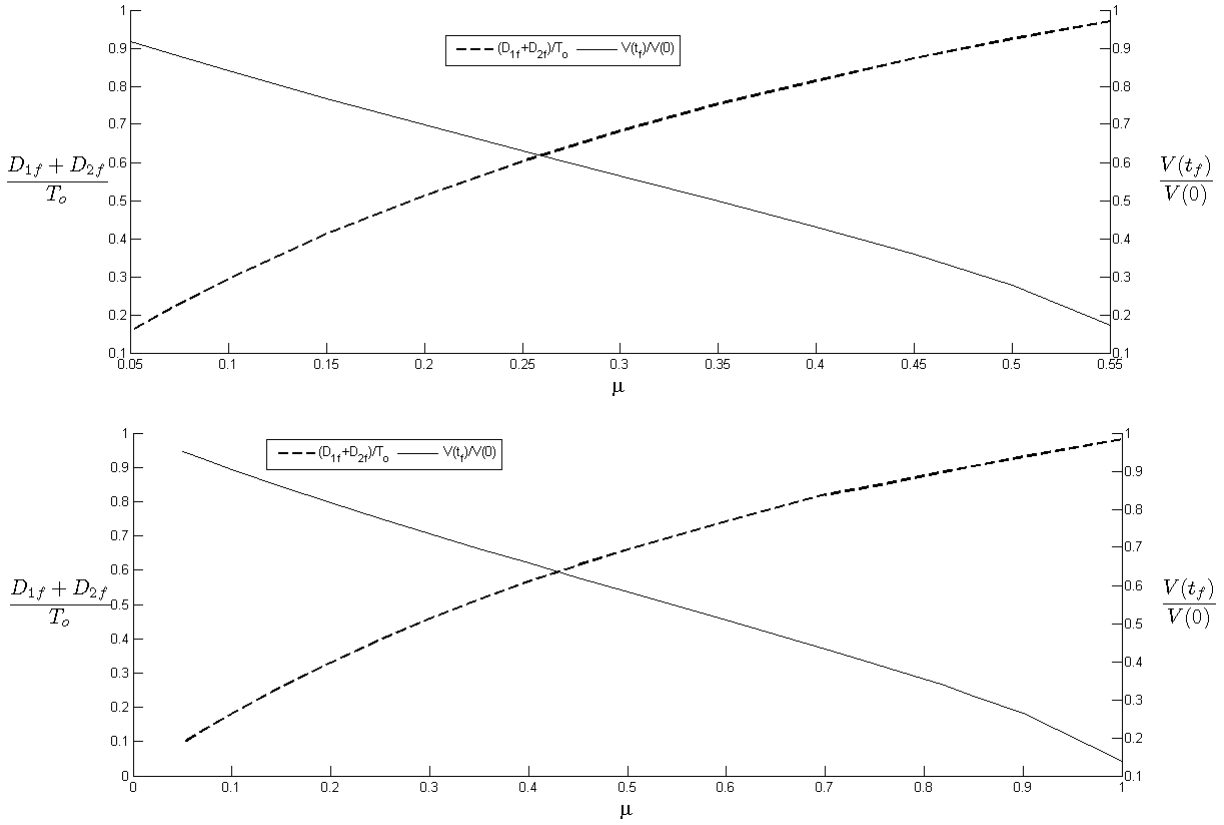

Figure 4.12: Frictional dissipation and final velocities during initially sliding impact of pendulum for different angles of impact, $\theta = 30$ and $45,^o$ top to bottom for $k_3/k_1 = 0.01$

during sticking friction force does not do any work since there is no sliding of contact point. During sticking, the only work done is as strain in the compliant elements and this energy is re-gained towards the end of the collision because of the perfectly elastic impact assumption. Hence, sticking phase is an energy preserving phase unlike sliding. On the other hand, according to rigid body approach, throughout the impact only sliding takes place. This means, the energy preserving behavior of sticking phase can not be included in the system of rigid body approach. The plot in Figure 4.13 for $\theta = 60^o$ shows for compliant cases final velocity to be the same as initial velocity for higher values of μ where gross sticking occurs.

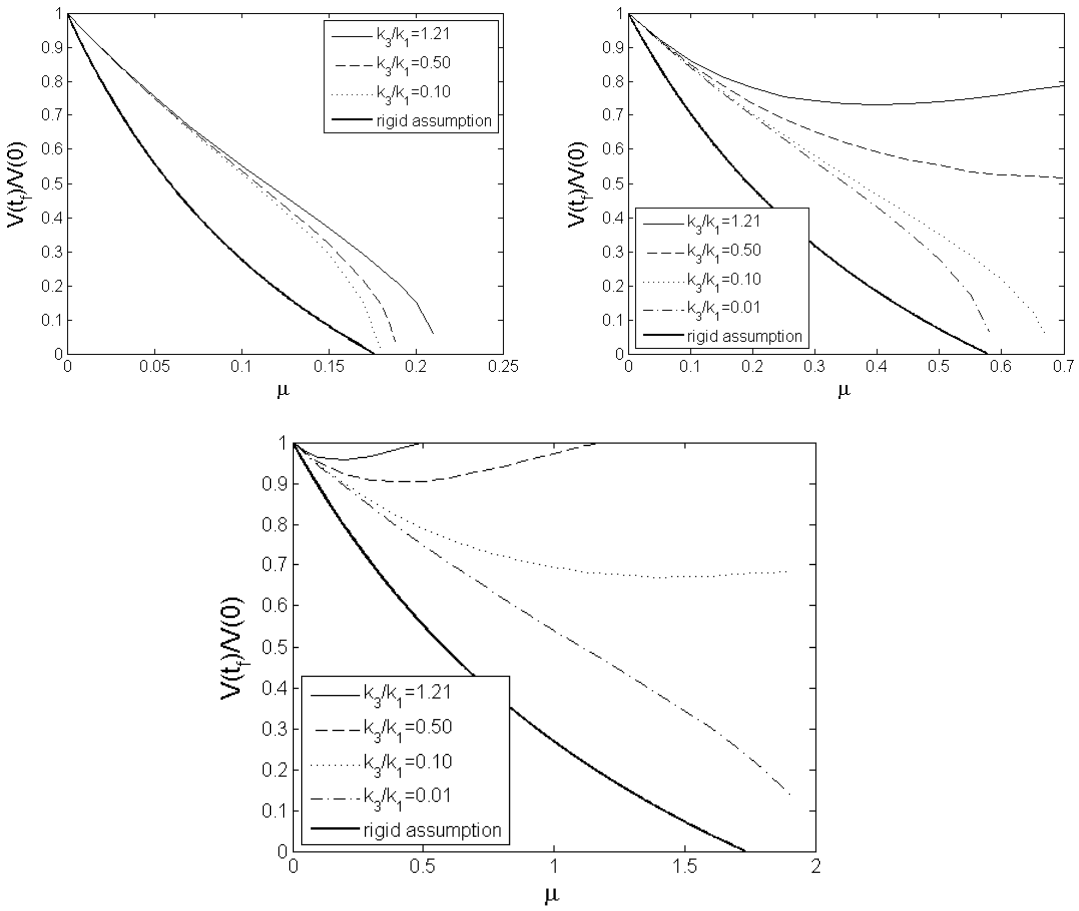

Figure 4.13: Comparison of compliant elements method to classical theory $\theta =$ 10, 30 and 60^o respectively

For the pendulum problem an additional possibility is observed during initially

sliding impact. In this case after t_{tl}, velocity of the pendulum goes to zero and the pendulum can not rebound. This condition will be analysed in more detail in the following section. Possibilities in an oblique impact is summarized in Figure 3.2.

4.2.1.5 Wedging

4.2.1.5.1 Wedging in Rigid Body Assumption Wedging (also referred to as cut-off or stick) is a term used for the condition where colliding bodies are not able to rebound at the end of an impact [1, 15, 36]. This is usually seen in constrained frictional eccentric impacts depending on the geometry of the system and friction between impacting bodies and has many implications on industrial applications such as locking of the system due to wedging especially in robotics.

Rigid pendulum model with negligible tangential compliance is frequently used in collision analysis resulting with $\mu > \tan\theta$ for wedging [1, 15, 36]. For example, Lubarda [36] reports that, if the friction coefficient is high enough and the angle of the pendulum at the start of the impact is low enough, pendulum wedges and does not rebound; referring to this angle as the critical angle with rigid body assumption, $\theta_{cr,r}$) . Other authors [1, 15, 36] find the limiting condition for this phenomenon using rigid body assumption. Writing the equation of motion about pivot point one can obtain impulse angular velocity relation [36]

$$\dot{\theta} = \dot{\theta}^{-} + \frac{x_o + \mu z_o}{J_o} P \qquad 0 \leq t \leq t_c$$

$$\dot{\theta} = \frac{x_o - \mu z_o}{J_o} (P - P_c) \qquad t_c \leq t \leq t_f \tag{4.70}$$

where subscript (c) denotes the time at the end of the compression phase and superscript (-) denotes initial value. In order that $\dot{\theta} > 0$, in the interval $t_c \leq t \leq t_f$, $x_o - \mu z_o > 0$ condition must be met which is the general result that is obtained in [1, 15, 36]. $\dot{\theta} > 0$ means pendulum has energy to rebound at the end of the impact, in other words $\dot{\theta} < 0$ means pendulum wedges (can not rebound), considering geometry this can be expressed as:

$$\mu > \tan\theta \tag{4.71}$$

4.2.1.5.2 Wedging with Compliant Elements at Contact For a given coefficient of friction, there is a limiting angle, θ_{cr}, where solution of the differential equation (3.49), used for the solution of sliding phase, diverges. The results are interpreted as the wedging conditions, since they demonstrate that both normal and tangential forces remain non-zero for an infinitely long time. The limiting condition for wedging using compliant elements model is a function of impact velocity, friction coefficient, ratio of normal and tangential stiffnesses, and θ.

For realistic values of k_3/k_1 (see Section 4.2.1.1.2), critical value of the impact angle, θ_{cr} is different than the critical angle calculated from rigid-body assumption. However as the ratio is decreased, i.e. tangential stiffness is increased, making the compliance smaller, θ_{cr} approaches to $\theta_{cr,r}$, where $\theta_{cr,r}$ is the critical angle calculated by rigid body approach given by Equation 4.71 as

$$\theta_{cr,r} = \tan^{-1}(\mu)$$

From Equation 4.71, impacting angles less than $\theta_{cr,r}$ causes wedging.

In Table 4.3 critical angles for increasing values of k_1 are presented for a physical pendulum. For $\mu = 1$, $\theta_{cr,r}$ is 45^o and it can be seen that as the compliance is decreased the system shows a rigid-like behavior.

k_3	k_1	θ_{cr}
1.5e7	$k_3/1.21$	11.69^o
1.5e7	$10\,k_3$	36.07^o
1.5e7	$100\,k_3$	43.90^o
1.5e7	$1000\,k_3$	44.89^o

Table 4.3: Limiting wedging angles with changing tangential stiffness for $\mu = 1$

For different friction coefficients, low tangential compliance shows similar results with the rigid body calculations and these values are presented in Table 4.4. Approach of θ_{cr} to $\theta_{cr,r}$ with decreasing compliance can be better seen From Figure 4.14 where critical angles with different friction coefficients for different stiffness ratios are presented.

Critical angle is calculated by a MATLAB code prepared for the physical

μ	k_3	k_1	$\theta_{cr,r}$	θ_{cr}
0.1	$1.5e7$	$1000\,k_3$	5.71	5.71
0.25	$1.5e7$	$1000\,k_3$	14.04	14.03
0.50	$1.5e7$	$1000\,k_3$	26.56	26.57
0.75	$1.5e7$	$1000\,k_3$	36.87	36.82
1.00	$1.5e7$	$1000\,k_3$	45.00	44.89

Table 4.4: Limiting wedging angles with changing coefficient of friction stiffness with

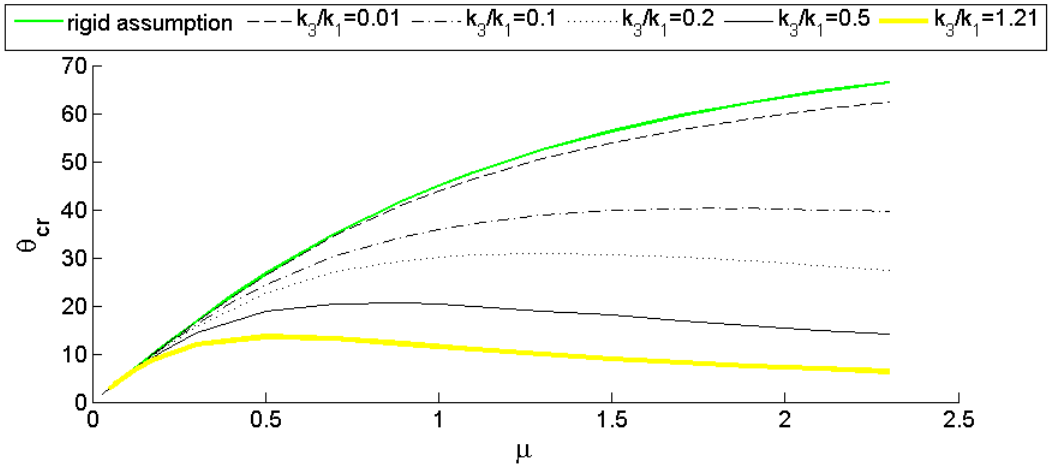

Figure 4.14: Critical angles for changing μ for different stiffness ratios

pendulum. As the collision angle θ, is decreased final velocities, $\dot{x}(t_f)$ and $\dot{z}(t_f)$, start to decrease. At a critical value of θ final velocities vanish. In collisions with smaller collision angles than the critical angle,θ_{cr}, both normal and tangential forces go to infinity. As an example, normalized forces for just above and below the critical impact angle are presented in Figure 4.15. The plot on the left-hand side shows a collision that rebounds. The plot on the right-hand side is an example of a wedged collision since contact forces persist for an infinite duration.

For wedging there is also a critical friction coefficient where wedging occurs for a specific value of k_3/k_1 and θ. In rigid body assumption, increasing the value of μ above the critical friction coefficient always causes wedging. However, with compliant elements model, this is not always the case. As an example, at $\theta = 13^o$ and $k_3/k_1 = 1.21$, for $0 < \mu < 0.4$ pendulum rebounds, values above 0.4 up to 0.7 causes wedging however above 0.7 pendulum can rebound again. This is

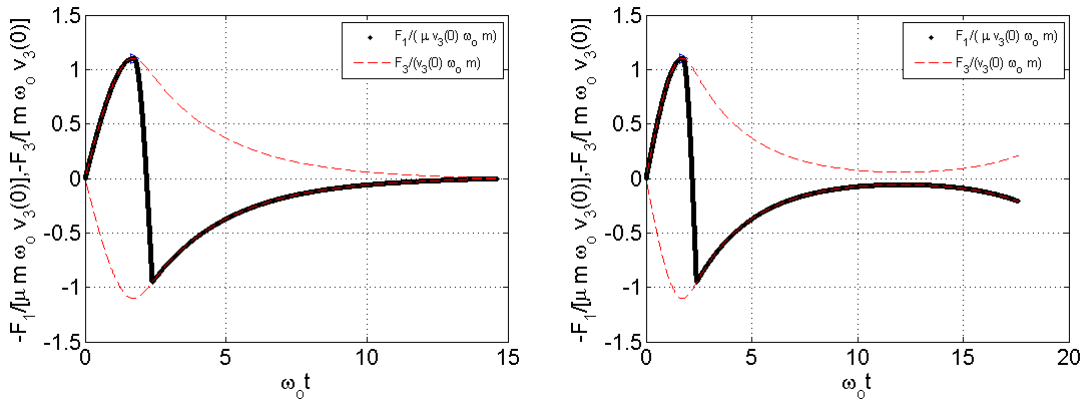

Figure 4.15: Forces above (left) and below θ_{cr} with $\mu = 1$, $k_3/k_1 = 0.1$, $\theta = 36.08^o$ and 36.07^o

illustrated in Figure 4.16. The plot on the left shows forces for $\mu = 0.1$, 0.5 and 1.0 and the result for $\mu = 0.5$ indicates wedging due to non-vanishing forces. This can also be seen from the velocity plot of Figure 4.16. If $\dot{x}/\dot{x}(0)$ of $\mu = 0.5$ is examined, it can be seen that initial and final directions of the tangential velocities are the same. For the pendulum, rebounding requires change of direction of the velocities because of the constrain. On the other hand, for $\mu = 0.8$, despite the increase in friction coefficient, signs of final and initial tangential velocities are different indicating rebound.

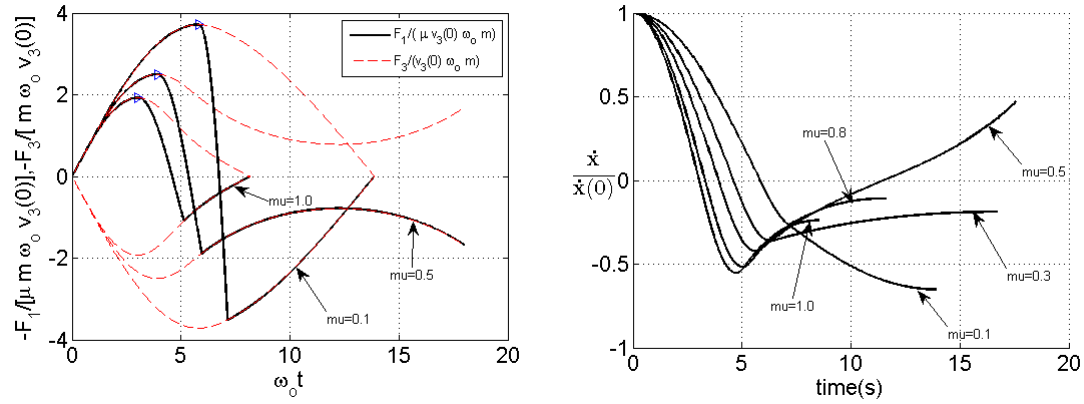

Figure 4.16: Wedging range for different μ, $k_3/k_1 = 1.21$ $\theta = 13^o$

On the other hand, this behavior is not encountered, for instance when $k_3/k_1 = 0.01$. As an example, $\theta = 26^o$ is taken since it is around the critical value. The calculations show that, up to $\mu = 0.4$ pendulum rebounds, but the

pendulum wedges any friction coefficient above this critical value unlike the previous case. Normalized forces and tangential velocities indicating this phenomenon are presented in Figure 4.17.

The variation of wedging limits with different stiffness ratios can be also seen in Figure 4.14. At high k_3/k_1 values θ_{cr} vs. μ curves show an increasing-decreasing trend whereas for low values of stiffness ratios θ_{cr} always increases with increasing μ and this can be explained by dissipation mechanism mentioned in Section 4.2.1.3. When Figure 4.11 and 4.12 compared it can be seen that for high values of k_3/k_1 maximum dissipation is at a intermediate μ value, where as for at low stiffness ratios dissipation increases with increasing μ.

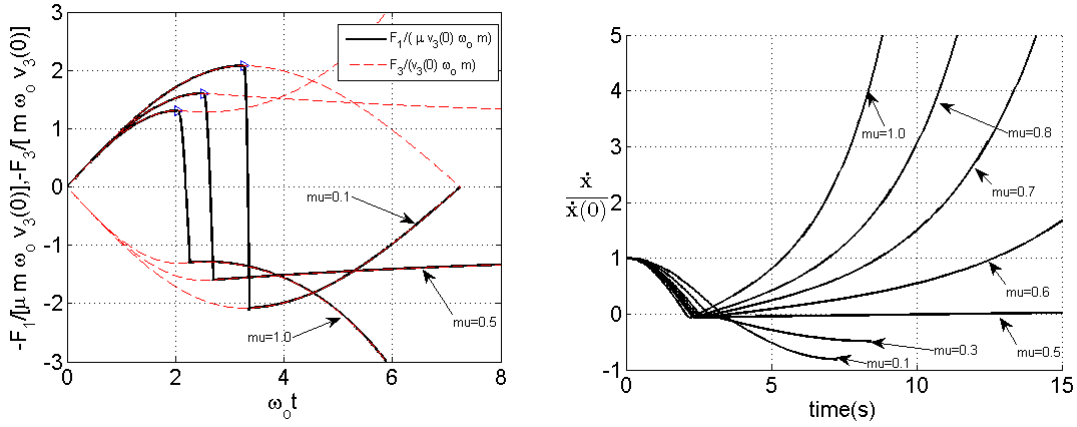

Figure 4.17: Wedging range for different μ, $k_3/k_1 = 0.01$ $\theta = 26^o$

Chapter 5

Conclusions

Constrained impact with friction is investigated using a pendulum colliding with a massive surface, by placing normal and tangential compliance elements between the contact point and the pendulum. To model contact, "deformable elements method" is preferred over the classical theory and continuum models since classical theory of impact may cause paradoxical energy increase in eccentric frictional impacts and a lack of information of forces, while continuum models are rather complicated and computationally expensive. Use of compliant models are generally accepted based on analytical derivations and experimental validations. As a result, effects of tangential compliance such as sticking or sliding state of the contact point, energy restoring phase of sticking can be seen with the model.

Compliant element model used here was constructed based on the impulse-momentum relations for 3D free impacts and an "effective" mass matrix, which relates impulse vector to the change of velocity vector. These relations are modified for a constrained collision example using a pendulum. By imposing the system constraints to the equations of motion, a relationship between velocity and impulse is obtained. To further investigate constrained impact with friction, a brief summary of impact with friction is presented. The wedging phenomenon that develops with the inclusion of friction in a constrained impact with rigid body assumption is also discussed.

Using the aforementioned topics as a basis for using compliant elements model, detailed description of the model is given with the mathematical relations. Equations obtained for dynamics of the collision is modified for sticking and sliding. During sticking, sliding velocity vanishes and hence tangential velocity of the pendulum and the rate of change of displacement of tangential compliant element become equal. This equality is used to obtain equations of motions for sticking. Similarly, during sliding, Amontons-Coulomb Law is used to obtain equations of motion describing sliding conditions. After obtaining the initiation conditions for either initially sliding or sticking case, options of transitions between these two modes of contact are discussed. The cases observed with using compliant element model, (i) initial sticking followed by sliding, (ii) gross sticking, (iii) initial sliding followed by sticking and sliding and (iv) gross sliding are discussed briefly.

The modes of impact and equations derived for a general planar impact are then modified for two examples: (i) oblique impact of a free sphere on a frictional massive surface, (ii) impact of a oblique slender rod on a frictional massive surface. The analysis of these two examples are discussed with force and velocity plots and explained considering their physical meaning.

Phenomena explained and equations derived thus far are used for a physical pendulum. After a brief review of the equations of motion, two phases of impact of the pendulum are explained in detail. Initially sliding collision of the pendulum showed dissimilar behavior compared free collision of sphere and rod examples. Unlike the examples of sphere and rod, sticking takes place throughout the entire impact period. Also, due to perfect elasticity assumption, final and initial velocities are equal preserving the initial energy of the system. Initially sliding pendulum behaves differently from the sphere and rod examples under some circumstances; the constraint in the system and friction causes locking of the system (wedging).

For a better understanding of the model with compliant elements at contact, effects of friction coefficient, μ, and impact angle, θ, are analysed. Different values of μ showed non-linear change in final velocities which showed increase of decrease with increasing μ, which lead to the investigation of energy dissipation

mechanisms in the system.

According to assumptions made, the only energy dissipation is from the presence of friction at contact. Calculations showed that, for high stiffness ratios, total energy loss of the system has a local minimum which means increasing μ does not always lead to increase in dissipation. On the other hand, at lower stiffness ratios dissipation increases with increase in μ.

To show the effect of tangential compliance, final velocities of the pendulum are compared with the ones that are calculated by classical impact theory using energetic coefficient of restitution. As the stiffness ratio decreases, the curves of final velocity vs. μ converge to a limiting curve, however, this curve shows significantly higher final velocities compared to the classical theory results. The reason for this difference is thought to be the missing sticking phase in the rigid contact model and consequently there is no energy dissipation, between initial and final sliding phases.

Finally, wedging of the pendulum is discussed in detail. The critical angle for wedging is compared with the critical angle calculated by rigid body assumption. It is seen that as the stiffness ratio is decreased, making the tangential compliance became more stiff, the values of critical angles reach a limiting value. These results are consistent with the results obtained by using rigid body model.

In summary, this thesis describes use of compliant elements to describe impact of a pendulum and analyzes its response considering, sliding and sticking phases of contact, dissipation mechanism, effect of several variables, and wedging. Although, there are several reports that present experimental results for free oblique impacts underlining significance of tangential compliance, experimental studies on constrained oblique collisions are scarce. Further studies to experimentally validate the present results would be helpful. Furthermore, deformable elements method can be extended by including material properties, developing more realistic contact models such as that by Hertz. Perfectly elastic collision assumption used in this thesis can be extended further by damping effects. Material damping could make a great example for such a dissipation model where time and collision dependent dissipation is included in the system.

Bibliography

[1] W. J. Stronge, "Friction in collisions: Resolution of a paradox," *Journal of Applied Physics*, vol. 69, no. 2, pp. 610–612, 1991.

[2] A. Ivanov, "On the problem of constrained collision," *Solid Mechanics and its Appliacations*, pp. 107–116, 1999.

[3] W. Stronge, "Planar impact of rough compliant bodies," *International journal of impact engineering*, vol. 15, no. 4, pp. 435–450, 1994.

[4] N. Maw, "The oblique impact of elastic spheres," *Wear*, 1976.

[5] W. J. Stronge, *Impact Mechanics*. cambridge: Cambridge University Press, 2000.

[6] G. Gilardi and I. Sharf, "Literature survey of contact dynamics modelling," *Mechanism and Machine Theory*, vol. 37, pp. 1213–1239, Oct. 2002.

[7] A. Ivanov, "The problem of constrained impact," *Journal of applied mathematics and mechanics*, vol. 61, no. 3, pp. 341–353, 1997.

[8] R. M. Brach, *Mechanical Impact Dynamics: Rigid Body Collisions*. New York: John Wiley Sons, 1991.

[9] M. Brach, "Classical Planar Impact Theory and the tip impact of a slender rod," *international journal of impact engineering*, vol. 13, no. 1, pp. 21–33, 1993.

[10] R. Brach, "Friction, restitution, and energy loss in planar collisions," *Journal of applied mechanics*, vol. 51, no. March, pp. 164–170, 1984.

[11] R. Brach, "Rigid body collisions," *Journal of Applied Mechanics*, vol. 56, no. March 1989, pp. 133–138, 1989.

[12] R. Brach, "Moments Between Impacting Rigid Bodies," *Journal of Mechanical Design*, vol. 103, no. October, pp. 812–817, 1981.

[13] R. Brach, "Formulation of rigid body impact problems using generalized coefficients," *International journal of engineering science*, vol. 36, no. 1, pp. 61–71, 1998.

[14] D. B. Marghitu and E. D. Stoenescu, "Rigid body impact with moment of rolling friction," *Nonlinear Dynamics*, vol. 50, pp. 597–608, Jan. 2007.

[15] F. Pfeiffer and C. Glocker, "Impacts with friction," p. Proc. of the 15th Biennial Conference on Mechanica, 1995.

[16] K. L. Johnson, *Contact Mechanics*. Cambridge: Cambridge University Press, 1985.

[17] W. Goldsmith, *Impact*. New York: Dover Publications, 1960.

[18] S. C. Hunter, "Energy absorbed by elastic waves during impac," *J Mech Phys Solids*, vol. 8, pp. 162–171, 1957.

[19] J. Reed, "Energy losses due to elastic wave propagation during an elastic impact," *Journal of Physics D: Applied Physics*, vol. 18, p. 23292337, 1985.

[20] R. Seifried, B. Hu, and P. Eberhard, "Numerical and experimental investigation of radial impacts on a half-circular plate," *Multibody System Dynamics*, vol. 9, pp. 265–281, 2003.

[21] R. Seifried and P. Eberhard, "Comparison of Numerical and Experimental Results for Impacts," in *Proceedings of the ENOC-2005 Fifth*, pp. 399–408, 2005.

[22] H. Hertz, "ber die Berhrung fester elastischer Krper," *J. reine angew. Math (Crelle)i*, vol. 92, 1881.

[23] R. D. Mindlin, "Compliance of elastic bodies in contact," *J. Appl. Mech.*, vol. 76, pp. 259–268, 1949.

[24] R. D. Mindlin and H. Deresiewicz, "Elastic spheres in contact under varying oblique forces," *J. Appl. Mech.*, pp. 327–344, 1953.

[25] N. Maw, J. Barber, and J. Fawcett, "The rebound of elastic bodies in oblique impact," *Mechanics Research Communications*, vol. 4, no. 1, pp. 17–22, 1977.

[26] N. Maw, J. Barber, and J. Fawcett, "The role of elastic tangential compliance in oblique impact," *J. Lubric. Technol.(Trans. ASME)*, vol. 103, no. January, pp. 74–80, 1981.

[27] J. Jaeger, "Analytical solutions of contact impact problems," *Applied Mechanics Reviews*, vol. 47, no. 2, pp. 35–54, 1994.

[28] P. P. Garland and R. J. Rogers, "An experimental study of contact forces during oblique elastic impact," *Journal of Applied Mechanics*, vol. 76, 2009.

[29] E. E. Osakue and R. J. Rogers, "An Experimental Study of Friction During Planar Elastic Impact," *Journal of Pressure Vessel Technology*, vol. 123, no. 4, pp. 493–500, 2001.

[30] W. J. Stronge, R. James, and B. Ravani, "Oblique impact with friction and tangential compliance," *Philosophical Transactions of the Royal Society A: Mathematical, Physical and Engineering Sciences*, vol. 359, pp. 2447–2465, Dec. 2001.

[31] E. T. Whittaker, *A tretise on the analytical dynamics of particles and rigid bodies*. cambridge: Cambridge University Press, 1904.

[32] R. M. Brach, *Philosophia naturalis principia mathematica*. London: Reg. Soc., 1686.

[33] W. Stronge, "Unraveling paradoxical theories for rigid body collisions," *Journal of Applied Mechanics*, vol. 58, no. December, pp. 1049–1055, 1991.

[34] Y. Wang and M. T. Mason, "Two-Dimensional Rigid-Body Collisions With Friction," *Journal of Applied Mechanics*, vol. 59, no. 3, p. 635, 1992.

[35] W. Stronge, "Rigid body collisions with friction," *Proceedings of the Royal Society of*, vol. 431, no. 1881, pp. 169–181, 1990.

[36] V. a. Lubarda, "The Bounds on the Coefficients of Restitution for the Frictional Impact of Rigid Pendulum Against a Fixed Surface," *Journal of Applied Mechanics*, vol. 77, no. 1, pp. 011006–1–011006–7, 2010.

[37] J. Batlle, "On Newton's and Poisson's rules of percussive dynamics," *Journal of applied mechanics*, vol. 60, no. 93, pp. 376–381, 1993.

[38] A. Ivanov, "Energetics of a collision with friction," *Journal of Applied Mathematics and Mechanics*, vol. 56, no. 4, pp. 624–631, 1992.

[39] J. Keller, "Impact with friction," *Journal of Applied Mechanics*, vol. 53, no. March, pp. 2–5, 1986.

[40] W. Stronge, "Swerve during three-dimensional impact of rough rigid bodies," *Journal of Applied Mechanics*, vol. 61, no. September, pp. 605–611, 1994.

[41] E. Berger, "Friction modeling for dynamic system simulation," *Applied Mechanics Reviews*, vol. 55, no. 6, pp. 535–577, 2002.

[42] D. P. Hess and A. Soom, "Normal Vibrations and Friction Under Harmonic Loads : Part I I Rough Planar Contacts," vol. 113, no. 90, pp. 87–92, 1991.

[43] H. M. Lankarani and P. E. Nikravesh, "A contact force model with hysteresis damping for impact analysis of multibody systems," *Journal of Mechanical Design*, vol. 112, no. September, pp. 369–376, 1990.

[44] K. Johnson, "One hundred years of Hertz contact," *Proc. Instn. Mech. Engrs.*, vol. 196, pp. 363–378, 1982.

[45] C. Zener, "The intrinsic inelasticity of large plates," *Physical Review*, vol. 59, pp. 669–673, 1941.

[46] P. Villaggio, "The rebound of an elastic sphere against a rigid wall," *Journal of applied mechanics*, vol. 63, no. June, pp. 259–263, 1996.

[47] W.-r. Chang and F. F. Ling, "Normal impact model of rough surfaces," *Journal of tribology*, vol. 114, no. July, pp. 439–447, 1992.

[48] P. P. Garland and R. J. Rogers, "An Analytical Solution for Shear Stress Distributions During Oblique Elastic Impact of Similar Spheres," *Journal of Computational and Nonlinear Dynamics*, vol. 3, no. 1, pp. 011002–1,011002–9, 2008.

[49] P. Kraus, A. Fredriksson, and V. Kumar, "Modeling of frictional contacts for dynamic simulation," in *Proceedings of IROS 1997 Workshop on Dynamic Simulation: Methods and Applications*, vol. 28, pp. 1–10, 1997.

[50] C. Lim and W. Stronge, "Oblique elasticplastic impact between rough cylinders in plane strain," *International Journal of Engineering Science*, vol. 37, pp. 97–122, Jan. 1999.

[51] D. Gugan, "Inelastic collision and the Hertz theory of impact," *American Journal of Physics*, vol. 68, no. 10, pp. 920–924, 2000.

[52] D. Gorham and a.H. Kharaz, "The measurement of particle rebound characteristics," *Powder Technology*, vol. 112, pp. 193–202, Oct. 2000.

[53] A. Seireg and E. Weiter, "Behavior of frictional hertzian contacts under impulsive loading," *Wear*, vol. 8, pp. 208–219, 1965.

[54] X. Shi and A. a. Polycarpou, "Measurement and Modeling of Normal Contact Stiffness and Contact Damping at the Meso Scale," *Journal of Vibration and Acoustics*, vol. 127, no. 1, p. 52, 2005.

[55] Y. Jia, "Energy-Based Modeling of Tangential Compliance in 3-Dimensional Impact," *Algorithmic Foundations of Robotics IX*, pp. 1–16, 2011.

[56] V. Bhatt and J. Koechling, "Classifying dynamic behavior during three dimensional frictional rigid body impact," in *Proceedings of the 1994 IEEE International Conference on Robotics and Automation*, pp. 2342–2348, IEEE Comput. Soc. Press, 1994.

[57] V. Bhatt and J. Koechling, "Partitioning the parameter space according to different behaviors during three-dimensional impacts," *Journal of applied mechanics*, vol. 62, no. September, pp. 740–746, 1995.

[58] V. Bhatt and J. Koechling, "Three-dimensional frictional rigid-body impact," *Journal of applied mechanics*, vol. 62, no. December, pp. 893–898, 1995.

[59] J. Batlle, "The sliding velocity flow of rough collisions in multibody systems," *Journal of applied mechanics*, vol. 63, no. September, pp. 804–809, 1996.

[60] Z. Zhen and C. Liu, "The analysis and simulation for three-dimensional impact with friction," *Multibody System Dynamics*, vol. 18, pp. 511–530, July 2007.

[61] I. Hutchings, N. Macmillan, and D. Rickerby, "Further studies of the oblique impact of a hard sphere against a ductile solid," *Int. J. Mech. Sci*, vol. 23, no. 11, pp. 639–646, 1981.